Monthly Notices of the ROYAL ASTRONOMICAL SOCIETY

MNRAS **462,** 876–892 (2016)
Advance Access publication 2016 July 15

doi:10.1093/mnras/stw1711

HD 24355 observed by the *Kepler K2* mission: a rapidly oscillating Ap star pulsating in a distorted quadrupole mode

Daniel L. Holdsworth,[1,2★] Donald W. Kurtz,[1] Barry Smalley,[2] Hideyuki Saio,[3] Gerald Handler,[4] Simon J. Murphy[5] and Holger Lehmann[6]

[1]*Jeremiah Horrocks Institute, University of Central Lancashire, Preston PR1 2HE, UK*
[2]*Astrophysics Group, Keele University, Staffordshire ST5 5BG, UK*
[3]*Astronomical Institute, School of Science, Tohoku University, Sendai 980-8578, Japan*
[4]*Copernicus Astronomical Center, Bartycka 18, PL-00-716 Warsaw, Poland*
[5]*Sydney Institute for Astronomy (SIfA), School of Physics, University of Sydney, NSW 2006, Australia*
[6]*Thüringer Landessternwarte Tautenburg (TLS), Sternwarte 5, D-07778 Tautenburg, Germany*

Accepted 2016 July 13. Received 2016 July 13; in original form 2016 May 6

ABSTRACT

We present an analysis of the first *Kepler K2* mission observations of a rapidly oscillating Ap (roAp) star, HD 24355 ($V = 9.65$). The star was discovered in SuperWASP broad-band photometry with a frequency of 224.31 d^{-1} (2596.18 μHz; $P = 6.4$ min) and an amplitude of 1.51 mmag, with later spectroscopic analysis of low-resolution spectra showing HD 24355 to be an A5 Vp SrEu star. The high-precision *K2* data allow us to identify 13 rotationally split sidelobes to the main pulsation frequency of HD 24355. This number of sidelobes combined with an unusual rotational phase variation show this star to be the most distorted quadrupole roAp pulsator yet observed. In modelling this star, we are able to reproduce well the amplitude modulation of the pulsation, and find a close match to the unusual phase variations. We show this star to have a pulsation frequency higher than the critical cut-off frequency. This is currently the only roAp star observed with the *Kepler* spacecraft in short cadence mode that has a photometric amplitude detectable from the ground, thus allowing comparison between the mmag amplitude ground-based targets and the μmag spaced-based discoveries. No further pulsation modes are identified in the *K2* data, showing this star to be a single-mode pulsator.

Key words: asteroseismology – techniques: photometric – stars: chemically peculiar – stars: individual: HD 24355 – stars: magnetic field – stars: oscillations.

1 INTRODUCTION

The rapidly oscillating Ap (roAp) stars are a rare subclass of the chemically peculiar, magnetic, Ap stars. They show pulsations in the range of 6–23 min with amplitudes up to 18 mmag in Johnson *B* (Holdsworth 2015), and are found at the base of the classical instability strip on the Hertzsprung–Russell (HR) diagram, from the zero-age main sequence to the terminal-age main sequence in luminosity. Since their discovery by Kurtz (1982), only 61 of these objects have been identified (see Smalley et al. 2015 for a catalogue). The pulsations are high-overtone pressure modes (p modes) thought to be driven by the κ-mechanism acting in the H I ionization zone (Balmforth et al. 2001). However, Cunha et al. (2013) have shown that turbulent pressure in the convective zone may excite some of the modes seen in a selection of roAp stars.

The pulsation axis of these stars is inclined to the rotation axis, and closely aligned with the magnetic one, leading to the oblique pulsator model (Kurtz 1982; Dziembowski & Goode 1985; Shibahashi & Saio 1985a,b; Shibahashi & Takata 1993; Takata & Shibahashi 1994, 1995; Bigot & Dziembowski 2002; Bigot & Kurtz 2011). Oblique pulsation allows the pulsation modes to be viewed from varying aspects over the rotation cycle of the star, giving constraints on the pulsation geometry that are not available for any other type of pulsating star (other than the Sun, which is uniquely resolved).

The mean magnetic field modulus in Ap stars is strong, of the order of a few kG to 34 kG (Babcock 1960). A strong magnetic field suppresses convection and provides stability to allow radiative levitation of some elements – most spectacularly singly and doubly ionized rare earth elements – producing a stratified atmosphere with surface inhomogeneities. These inhomogeneities, or spots, are long-lasting (decades in many known cases) on the surface of Ap stars, thus allowing for an accurate determination of the rotation period of the star. In the spots, rare earth elements such as La, Ce, Pr, Nd, Sm, Eu, Gd, Tb, Dy and Ho may be overabundant by up to a million

★ E-mail: dlholdsworth@uclan.ac.uk

© 2016 The Authors
Published by Oxford University Press on behalf of the Royal Astronomical Society

Downloaded from http://mnras.oxfordjournals.org/ at Keele University on August 15, 2016

times the solar value, leading to spectral line strength variations over the rotation period (e.g. Lüftinger et al. 2010). Because of the complex atmospheres of the Ap stars, the roAp stars provide the best laboratory, beyond the Sun, to study the interactions between pulsations, rotation and chemical abundances in the presence of magnetic fields.

Early photometric campaigns targeted known Ap stars in the search for oscillations (e.g. Martinez, Kurtz & Kauffmann 1991; Martinez & Kurtz 1994), with later studies using high-resolution spectroscopy to detect line profile variations in Ap stars caused by pulsational velocity shifts (e.g. Savanov, Malanushenko & Ryabchikova 1999; Kochukhov & Ryabchikova 2001; Hatzes & Mkrtichian 2004; Mkrtichian et al. 2008; Elkin et al. 2010; Elkin, Kurtz & Mathys 2011; Kochukhov et al. 2013). Most recently, the use of the SuperWASP (Wide Angle Search for Planets) ground-based photometric survey led to the identification of 11 roAp stars (Holdsworth et al. 2014a; Holdsworth 2015).

With the launch of the *Kepler* space telescope, the ability to probe to μmag precision has enabled the detection of four roAp stars with amplitudes below the ground-based detection limit: KIC 8677585 was a known A5p star observed during the 10-d commissioning phase of the *Kepler* mission and was shown to pulsate by Balona et al. (2011a); KIC 10483436 (Balona et al. 2011b) and KIC 10195926 (Kurtz et al. 2011) were identified as roAp stars through analysis of their light curves and subsequent spectra; KIC 4768731 was identified as an Ap star by Niemczura et al. (2015) and was later shown to be a roAp star (Smalley et al. 2015). Finally, *Kepler* observations also allowed the analysis of one roAp star, KIC 7582608, identified in the SuperWASP survey with an amplitude of 1.45 mmag (Holdsworth et al. 2014b), albeit in the super-Nyquist regime (Murphy, Shibahashi & Kurtz 2013).

There is an obvious difference between the roAp stars discovered with ground-based photometry and those first detected by space-based observations: the amplitudes of the pulsations in the ground-based discoveries are generally in the range 0.5–10 mmag, whereas the *Kepler* observations did not detect variations above 0.5 mmag. Ground-based observations are usually made in the *B* band where the pulsation amplitude is greatest for the roAp stars (Medupe & Kurtz 1998), and *Kepler* observations are made in a broad-band, essentially white, filter where the amplitudes may be a factor of 2–3 lower. This accounts for some of the difference between the two groups. Further to this, ground-based observations are limited due to white noise caused by sky transparency variations in the frequency range in which roAp stars are observed to pulsate, thus affecting the minimum amplitude that can be detected, suggesting that this may be an observational bias. However, the question remains as to whether there is a fundamental difference between the two groups. Are the differences in amplitude solely due to selection effects, or do the stars show differences in their abundance anomalies, magnetic field strengths, ages or rotation rates? The observations at μmag precision of a roAp star discovered with ground-based photometry may begin to provide insight into this disparity.

Ground-based projects in the search for transiting exoplanets produce vast amounts of data on millions of stars (e.g. OGLE, Udalski et al. 1992; ASAS, Pojmanski 1997; HATnet, Bakos et al. 2004; WASP, Pollacco et al. 2006; KELT, Pepper et al. 2007). These data can provide an excellent source of information on many thousands of variable stars. Indeed, many of these projects have been employed for that purpose (e.g. Pepper et al. 2008; Hartman et al. 2011; Ulaczyk et al. 2013; Holdsworth et al. 2014a). The ability of these surveys to achieve mmag precision provides an extensive all-sky data base in which to search for low-amplitude stellar variability, which can then be observed at much higher precision by space-based missions such as *K2* (Howell et al. 2014) and *TESS* (Ricker et al. 2015).

One of the leading ground-based projects in the search for transiting exoplanets, which provides data for many millions of stars, is the SuperWASP survey. This project is a two-site, wide-field survey, with instruments located at the Observatorio del Roque de los Muchachos on La Palma (WASP-N) and the Sutherland Station of the South African Astronomical Observatory (WASP-S; Pollacco et al. 2006). Each instrument has a field of view of ∼64 deg^2, with a pixel size of 13.7 arcsec. Observations are made through a broad-band filter covering a wavelength range of 4000–7000 Å and consist of two consecutive 30-s integrations at a given pointing, with pointings being revisited, typically, every 10 min. The data are reduced with a custom reduction pipeline (see Pollacco et al. 2006) resulting in a 'WASP *V*' magnitude which is comparable to the Tycho-2 V_t passband. Aperture photometry is performed at stellar positions provided by the USNO-B1.0 input catalogue (Monet et al. 2003) for stars in the magnitude range $5 < V < 15$.

As previously mentioned, one of the space-based missions which ground-based surveys can inform is the *K2* mission. After the failure of a second of four reaction wheels, the *Kepler* spacecraft could no longer maintain its precise pointing towards the original single field of view. The loss of the reaction wheels now means that the spacecraft needs to account for the solar radiation pressure in a new way. This has been achieved by pointing the telescope in the orbital plane. This new configuration requires semi-regular ∼5.9-h drift corrections, as well as momentum dumps through thruster firings every few days (Howell et al. 2014). To avoid sunlight entering the telescope, a new field is selected every approximately 80 d. Such a procedure has led to the fields being labelled as 'Campaigns'.

Due to the shutterless exposures of the *Kepler* spacecraft, the pointing drift leads to changes in brightness of an observed star as it moves across the CCD. There exist several routines to perform corrections on a large scale (e.g. Handberg & Lund 2014; Vanderburg & Johnson 2014) which aim to reduce the systematic noise in the light curve and resultant periodogram. With careful reduction of the raw *K2* data, the science data give a photometric precision within a factor of 3–4 of that of *Kepler* for a 12th magnitude G star (Howell et al. 2014).

The re-purposing of the *Kepler* spacecraft has opened up a host of new possibilities to observe variable stars at μmag precision. The changing field of view now allows the study of O-type stars (Buysschaert et al. 2015), the prospect of detecting semi-convection in B-type stars (Moravveji 2015), observations of variable stars in nearby open clusters (Nardiello et al. 2015), observations of RR Lyrae stars beyond the Galaxy (Molnár et al. 2015) and now the first observations, in short cadence (SC), of a classical, high-amplitude, roAp star.

HD 24355 is a bright ($V = 9.65$) roAp star, discovered by Holdsworth et al. (2014a). Their data show a pulsation at 224.31 d^{-1} (2596.18 μHz; $P = 6.4$ min) with an amplitude of 1.51 mmag in the WASP broad-band filter. In this paper, we present a detailed spectral classification followed by an in-depth discussion of the SuperWASP discovery data, alongside further ground-based observations. We then present an analysis of the *K2* Campaign 4 data.

2 SPECTRAL CLASSIFICATION

We obtained two classification resolution spectra of HD 24355 (Fig. 1). The first, published in Holdsworth et al. (2014a), was taken on 2012 October 25 with the Intermediate dispersion

Downloaded from http://mnras.oxfordjournals.org/ at Keele University on August 15, 2016

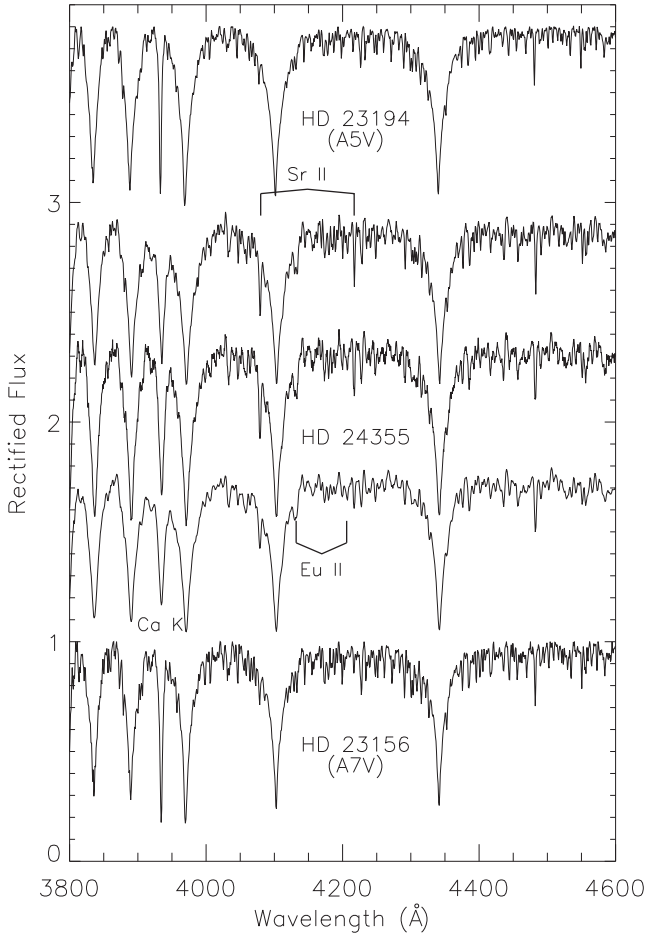

Figure 1. Spectra of HD 24355 (the three central spectra) compared with two MK standard stars of A5 and A7 type. Note the strong lines of Sr II at 4077 and 4216 Å and the enhanced lines of Eu II at 4130 and 4205 Å in the target star. The upper spectrum for HD 24355 was obtained with the ANU/WiFeS instrument, the second with the WHT/ISIS instrument, with the lower obtained with the LAMOST instrument. The spectra have been ordered in rotation phase and offset for clarity.

Spectrograph and Imaging System (ISIS) mounted on the 4.2-m William Herschel Telescope (WHT), at a resolution of $R \sim 2000$. The second spectrum was obtained on 2014 November 15 using the Wide-Field Spectrograph (WiFeS) mounted on the 2.3-m Australian National University (ANU) telescope at Siding Spring Observatory at a resolution of $R \sim 3000$.

The ISIS data were reduced using the FIGARO package (Shortridge et al. 2004), which is part of the STARLINK[1] suite of programs. The WiFeS data were reduced with the PYWIFES software package (Childress et al. 2014).

In addition to our data, HD 24355 has been observed as part of the LAMOST campaign (Cui et al. 2012; Zhao et al. 2012) and was made public as part of Data Release 1 (Luo et al. 2015). The LAMOST spectrum was obtained at a resolution of $R \sim 1800$, and is shown in Fig. 1 alongside the other spectra. Furthermore, in addition to classification spectra, we have obtained high-resolution, $R \sim 58\,000$, spectra using the coudé échelle spectrograph mounted on the 2.0-m telescope at the Thüringer Landessternwarte (TLS) Tautenburg, Germany, which we discuss in Section 3. Table 1 gives details of all spectral observations. The phases have been calculated relative to the second pulsational maximum in the *K2* data set, such that

$$\phi(E) = 2457108.8867 + 27\overset{\mathrm{d}}{.}9158 \times E, \quad (1)$$

where E is the number of rotation cycles elapsed since the reference time.

Table 1. Observation details for the all spectra. The S/N was determined using the DER_SNR code of Stoehr et al. (2008). The rotation phase has been calculated from equation (1), as shown in the text.

Instrument	BJD−2450000.0	Exposure time (s)	S/N	Resolution	Rotation phase
ISIS	6225.6426	15	50	2000	0.360
LAMOST	6295.0420	2400	80	1800	0.846
WiFeS	6977.1331	300	30	3000	0.280
TLS	7375.5077	2400	70	58 000	0.551
TLS	7380.4749	2400	65	58 000	0.729

Following the classification process described by Gray & Corbally (2009), we see that the Balmer line types are close matches to the A5 and A7 MK standard stars[2] (HD 23194 and HD 23156, respectively) with many of the metal lines being well matched by the standard A5 star. There are, however, peculiarities which do not match the standard stars. Both spectra show strong enhancements of Sr II at 4077 and 4216 Å, and Eu II at 4130 and 4205 Å. While the Eu II line at 4130 Å can be blended with a Si II doublet at 4128 and 4131 Å, we see no sign of Si II at 3856 and 3862 Å, which are used to confirm the Si peculiarity in Ap stars. Lines of Cr II at 3866, 4111and 4172 Å are not enhanced when compared to the MK standard stars, ruling out Cr peculiarities. With the obvious presence of Sr II and Eu II lines in the spectra, we conclude that HD 24355 is an A5Vp SrEu star.

The Ca II K line is also abnormal in this star, a common trait in the Ap stars. The line is much broader and shallower than those of the standard stars. As the broadening is apparent in just this single line, we attribute the abnormality to chemical stratification in the atmosphere in the presence of a magnetic field, similar to that shown by Smalley et al. (2015); comparison between a model atmosphere and a high-resolution spectrum is needed to confirm this. There is no clear difference between the line strengths of the peculiar lines between the two spectra, but given the relatively small shift in rotation phase between them, this is not unexpected.

We derive an effective temperature for HD 24355 by fitting the Balmer lines of our spectra. Given their low resolution, we are unable to determine a $\log g$ of the star, so fix this value at 4.0 which is a reasonable approximation for this exercise. From the WiFeS spectrum, we derive $T_{\mathrm{eff}} = 8200 \pm 250$ K and from the ISIS data we find $T_{\mathrm{eff}} = 8200 \pm 200$ K.

The LAMOST spectra are automatically analysed by instrument-specific software to determine fundamental parameters of the star. For HD 24355, the pipeline suggests $T_{\mathrm{eff}} = 8638 \pm 100$ K, $\log g = 4.15 \pm 0.41$ (cgs) and $[\mathrm{Fe/H}] = 0.7 \pm 0.22$. However, when trying to fit these parameters to the spectrum, we find a large disparity. Given the resolution of the spectrum, we are unable to determine a revised $\log g$ (so we set this to 4.0 as above). We find that $T_{\mathrm{eff}} = 8150 \pm 250$ K fits the Balmer lines much better than the higher

[1] http://starlink.jach.hawaii.edu/starlink

[2] Spectra of the standard stars were obtained from R. O. Gray's website: http://stellar.phys.appstate.edu/Standards/std1_8.html

Downloaded from http://mnras.oxfordjournals.org/ at Keele University on August 15, 2016

value of the LAMOST estimate, and 8150 ± 250 K is in agreement with the other two spectra.

3 SPECTRAL ANALYSIS

To analyse HD 24355 in detail, we obtained two high-resolution spectra with the coudé échelle spectrograph mounted on the 2.0-m telescope at the TLS Tautenburg, Germany. These spectra have a resolution of $R = 58\,000$, and cover a wavelength range from 4720 to 7360 Å. They were reduced using the standard ESO MIDAS packages. Information about the spectra is given in Table 1.

To determine the $T_{\rm eff}$ and $\log g$ of HD 24355, we measured the equivalent widths of 60 Fe I lines and 41 Fe II lines using UCLSYN (Smith & Dworetsky 1988; Smith 1992; Smalley, Smith & Dworetsky 2001). The effective temperature was found to be 8700 ± 100 K by requiring no dependence of abundance with excitation potential. For the $\log g$ determination, we tested the ionization balance between Fe I and Fe II, finding $\log g = 4.2 \pm 0.2$ (cgs).

The Fe abundance measured from the 101 lines is $\log A({\rm Fe}) = 8.3 \pm 0.3$, indicating an overabundance relative to solar of [Fe/H] = 0.8 dex, based on the solar chemical composition presented by Asplund et al. (2009).

We also use the Fe lines to establish the microturbulence velocity of HD 24355. We require no trend between the calculated abundances and their equivalent width when the correct value of microturbulence is chosen. We find that a low value (∼0.0 km s^{-1}) of microturbulence provides us with no trend.

Finally, we determine that the $v \sin i$ of HD 24355 is low by fitting lines with a series of synthetic spectra with varying $v \sin i$ values. We derive an upper limit of 3.5 km s^{-1}. Although this is below the quoted resolution of the spectrum, as lines sample more than one resolution element, it is possible to attain a sub-element velocity measurement. We provide an upper limit as we have not accounted for the effects of magnetic broadening or macroturbulence.

As well as using the spectra to determine the $T_{\rm eff}$ of HD 24355, we have performed spectral energy distribution (SED) fitting. We use literature photometry from 2MASS (Skrutskie et al. 2006), B and V magnitudes from Høg et al. (1997), USNO-B1 R magnitude (Monet et al. 2003), CMC14 r' from Evans, Irwin & Helmer (2002) and the TASS I magnitude (Droege et al. 2006) to reconstruct the SED. There is no evidence in our high-resolution spectra of interstellar reddening along the line of sight to HD 24355.

The stellar $T_{\rm eff}$ value was determined by fitting an $[M/{\rm H}] = +0.5$ Kurucz (1993) model to the SED. The model fluxes were convolved with photometric filter response functions. A weighted Levenberg–Marquardt non-linear least-squares fitting procedure was used to find the solution that minimized the difference between the observed and model fluxes. We used a $\log g = 4.0 \pm 0.5$ for the fit. The uncertainty in $T_{\rm eff}$ includes the formal least-squares error and adopted uncertainties in $\log g$ of ±0.5 and $[M/{\rm H}]$ of ±0.5 added in quadrature. As a result of the SED fitting, we derive a temperature of 7290 ± 180 K.

It is clear that the methods used provide a wide range of $T_{\rm eff}$ values for HD 24355 (8638 ± 100 K, LAMOST; 8200 ± 200 K, Balmer fitting; 8700 ± 100 K, Fe lines; 7100 ± 120 K, SED). This is similar to the Ap star 53 Cam (Kochukhov et al. 2004). In their analysis, they used different methods to determine the $T_{\rm eff}$ and $\log g$ of the star, and arrive at different values. They conclude that flux redistribution and line blanketing (Pyper & Adelman 1983) and vertical gradients in elemental abundances (Wade et al. 2003) are the major causes in their discrepancies. These factors, as well as the use of inaccurate metallicities in the synthetic spectrum, may account for the disparities in our measurements. We also note that we do not take into account the effects of the magnetic field when we derive our $T_{\rm eff}$, which can affect the result.

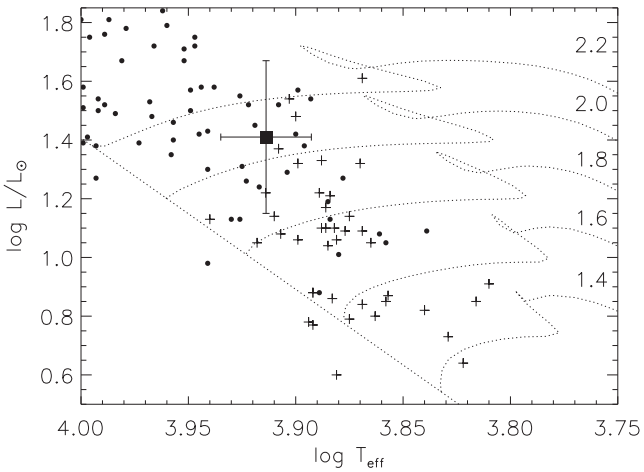

Figure 2. The position of HD 24355 on the HR diagram, as derived from the spectra. The other roAp stars (pluses) and the noAp stars (circles) are also shown for context. The zero-age main sequence and evolutionary tracks are from Bertelli et al. (2008).

In the case of HD 24355, we have shown the LAMOST derived temperature to be an overestimate based on the Balmer lines. The temperature derived from the SED fitting is much below that derived from the Balmer lines and is perhaps undersampled with the available photometry combined with flux redistribution due to line blanketing. Stratification is a well-known phenomenon in Ap stars, and as such we suspect this is also the case here, where we have attempted to use the Fe lines to derive the temperature. Therefore, based on the Balmer lines of both the high- and low-resolution spectra, we derive $T_{\rm eff} = 8200 \pm 250$ K for HD 24355. At this temperature (and with the associated error), it is not possible to constrain the value of $\log g$, and we therefore assume a value of 4.0 ± 0.2 (dex).

Using the relations of Torres, Andersen & Giménez (2010), and our values of $T_{\rm eff} = 8200 \pm 200$, $\log g = 4.0 \pm 0.2$ and [Fe/H] = 0.8 ± 0.3, we are able to derive the following parameters of the star: $M = 2.40 \pm 0.38\,{\rm M}_\odot$, $R = 2.53 \pm 0.43\,{\rm R}_\odot$. From these, we calculate the star's luminosity to be $\log(L/{\rm L}_\odot) = 1.41 \pm 0.26$. These parameters then allow us to plot HD 24355 on an HR diagram, as shown in Fig. 2, alongside other roAp stars and non-oscillating Ap (noAp) stars.

3.1 Magnetic field

Analyses of the two high-resolution spectra show there to be no magnetic splitting of spectral lines in this star. Therefore, to estimate the magnetic field strength, we use the method of Mathys & Lanz (1992). The ratio of strengths of Fe II 6147.7 to 6149.2 Å can be used as a proxy to estimate the mean magnetic field strength $\langle B \rangle$. Using the relative intensities of the lines, we measure a relative intensification of $\Delta W_\lambda / \overline{W}_\lambda$ to be 0.00 ± 0.02 and 0.08 ± 0.02 for the two spectra, respectively. Taking the mean of these measurements, and using the relation in Mathys & Lanz (1992), this provides us with a mean magnetic field modulus of 2.12 ± 1.44 kG. However, it is noted by Mathys & Lanz (1992) that the relation used cannot be extrapolated to weak fields, as is the case here, due to the different

Downloaded from http://mnras.oxfordjournals.org/ at Keele University on August 15, 2016

Table 2. The abundances of the rare earth elements in HD 24355. Abundances are given in the form $\log A(\mathrm{El}) = \log(N_{\mathrm{EL}}/N_{\mathrm{H}}) + 12$. The second column, n, denotes the numbers of lines used to derive the abundance. The errors are the standard deviations of the n measurements, and the solar abundances are from Asplund et al. (2009) for reference.

El	n	$\log A(\mathrm{El})$	Solar
La	5	3.14 ± 0.34	1.10
Ce	4	3.47 ± 0.33	1.58
Pr	8	3.17 ± 0.66	0.72
Nd	16	4.02 ± 0.97	1.42
Sm	3	3.10 ± 0.53	0.96
Eu	5	2.78 ± 0.56	0.52
Gd	6	3.47 ± 0.26	1.07
Tb	3	3.42 ± 0.10	0.30
Dy	2	3.18 ± 0.19	1.10
Er	3	3.13 ± 0.29	0.92
Tm	1	3.3	0.10
Yb	5	3.59 ± 0.24	0.84
Lu	3	1.93 ± 0.15	0.10

rate at which the two Fe II lines desaturate. We therefore treat this result only as an indication on the upper limit to the field strength.

3.2 Identification of rare earth elements

In Table 2, we provide a first measurement of the rare earth element abundances in HD 24355. As the two TLS spectra were obtained at similar rotation phases, we have co-added the two spectra and used the UCLSYN package (Smith & Dworetsky 1988; Smith 1992; Smalley et al. 2001) to measure a selection of isolated rare earth element lines in the spectrum. As the table shows, there is a significant overabundance of the rare earth elements in HD 24355 when compared to the solar values, with some elements still enhanced when compared to other roAp stars (e.g. Bruntt et al. 2008; Elkin et al. 2011; Smalley et al. 2015).

4 PHOTOMETRY

The pulsation in HD 24355 was discovered by Holdsworth et al. (2014a) after conducting a survey of the SuperWASP archive in a search for pulsating A stars. Here we provide a more detailed discussion of the discovery data, with the addition of further ground-based data obtained with the 0.75-m Automatic Photoelectric Telescope (APT) at Fairborn Observatory in Arizona, USA. Furthermore, we present the first SC data of a roAp star from the re-purposed *Kepler* space telescope, *K2*. HD 24355 is the only Ap star observed in *Kepler's* SC mode whose rapid oscillations have high enough amplitude to be observed from the ground.

4.1 Ground-based observations

4.1.1 SuperWASP

SuperWASP observed HD 24355 for three seasons, 2006, 2009 and 2010. The data were passed through a resistant mean algorithm to remove outlying points to improve the quality of the periodogram; see Holdsworth et al. (2014a) for an example and details. After trimming the data, there were 7951 data points remaining.

The light curve shows a clear signature at low frequency that is indicative of rotation (Fig. 3). The stable spots on Ap stars are usually aligned with the magnetic axis, which in turn is inclined to the rotation axis, leading to the rigid rotator model of Stibbs (1950), which manifests itself as a variation in brightness as the star rotates. As such, the rotation period of the star can be determined. Using the PERIOD04 program (Lenz & Breger 2005), we detect a peak in the periodogram at a frequency of $0.071\,6439 \pm 0.000\,0057$ d^{-1} ($P = 13.9579 \pm 0.0011$ d), where the error is the analytical error given in PERIOD04, using the method of Montgomery & O'Donoghue (1999). However, when combining all seasons of WASP data to calculate the rotation period, there is evidence of a sub-harmonic to that frequency. We therefore simultaneously calculate the peak at 0.0716 d^{-1} and a frequency at half that value, namely 0.035 8219 d^{-1}. In doing so, we are able to find a more precise measure of the rotation frequency and its harmonic. We find $\nu = 0.071\,6439 \pm 0.000\,0063$d^{-1} and $\nu/2 = 0.035\,8220 \pm 0.000\,0032$, corresponding to periods of 13.9579 ± 0.0011 d and 27.9158 ± 0.0025 d, respectively. In these ground-based survey data, differentiating between the rotation frequency and any harmonics can be problematic as low-amplitude peaks can be lost in the noise, especially in individual data sets. We therefore confirm the true rotation frequency with the *K2* data, in Section 4.2.

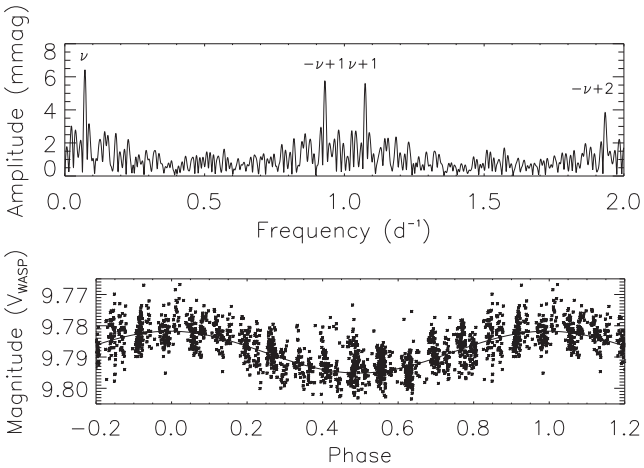

Figure 3. Top: low-frequency periodogram of the SuperWASP light curve from 2010 showing what was thought to be the rotation frequency of the star, as well as its positive and negative aliases. Bottom: SuperWASP phase folded light curve on the frequency determined in the upper panel, i.e. $\nu 0.071\,65$ d^{-1}. The plot shows a clear single sinusoidal signature with a period of $1/\nu = 13.9558$ d. Analysis of the *Kepler* data in Section 4.2.2 shows that the true rotation period is twice this value. The data have been binned to 5:1.

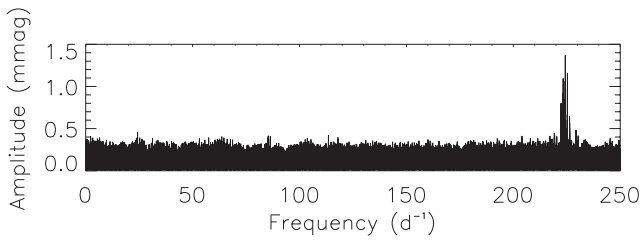

Figure 4. Periodogram of all seasons of WASP data. The data have been pre-whitened to 10 d^{-1} to the approximate noise level of the high-frequency range to remove the rotation signature and low-frequency noise. Note that the structure surrounding the pulsation signature is a result of daily aliases.

The pulsation signature of HD 24355 is apparent in all seasons of data, and is shown in Fig. 4. Each season of data has been pre-whitened, to 10 d^{-1}, to the approximate noise level of the

Downloaded from http://mnras.oxfordjournals.org/ at Keele University on August 15, 2016

Table 3. Details of the WASP observations, and the results of a non-linear least-squares fit of the pulsation frequency in each of the seasons. BJD is given as BJD−2450000.0, and the zero-point for the phases is taken to be the mid-point of the individual data sets.

Season	BJD start	Length (d)	Number of points	Frequency (d^{-1})	Amplitude (mmag)	Phase (rad)
2006	3995.5894	129.7952	2083	224.3073±0.0004	1.89±0.18	2.391 ± 0.089
2009	5148.4549	83.0317	1847	224.3048±0.0007	1.39±0.17	−2.415 ± 0.124
2010	5470.5701	125.9043	4021	224.3052±0.0004	1.55±0.12	−2.201 ± 0.077

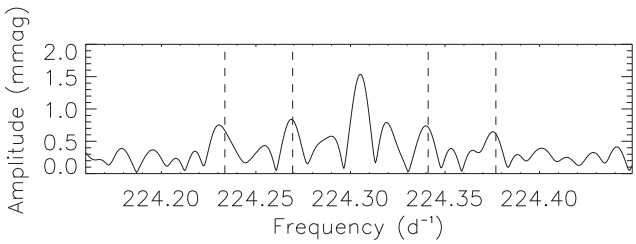

Figure 5. SuperWASP detections of sidelobes to the pulsation frequency in the 2010 season. The sidelobes are approximately at frequencies ±1 and ±2 times the rotational sub-harmonic frequency (as shown by the dashed lines). This suggests that the rotation frequency is 0.0358 d^{-1} i.e. a period of 27.9117 d.

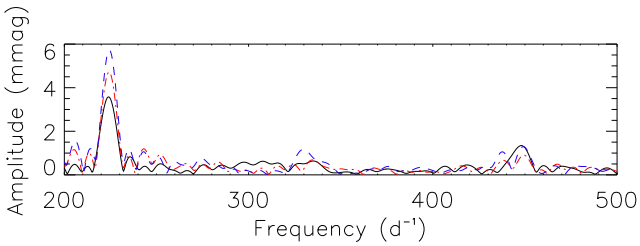

Figure 6. Periodograms of the three nights of APT data. There is a clear increase in the pulsation amplitude as the nights progress, from the solid black line, to the dot–dashed red line, to the dashed blue line. Also evident is the harmonic at twice the pulsation frequency.

high-frequency range to remove the rotation signature and the remaining low-frequency 'red' noise after the data have been processed by the WASP pipeline (Smith et al. 2006). The pulsation is clearly seen at a frequency of 224.3071 d^{-1} with an amplitude of 1.51 mmag in the WASP passband. The frequencies, amplitudes and phases of a non-linear least-squares fit for each season are provided in Table 3.

Due to the survey nature of this ground-based data set, not much further information can be extracted: the noise level in the high-frequency range is too great to discern, with confidence, sidelobes of the pulsation split by the rotation frequency. However, in the 2010 season of data, there do appear to be peaks split from the pulsation by the sub-harmonic of the strongest low-frequency peak (Fig. 5). This provides evidence that the rotation period is likely to be of the order of 27 d rather than 13 d. Again, analysis of the *K2* data in the following section resolves this disparity.

4.1.2 0.75-m APT

We observed HD 24355 for 3 h on each of three consecutive nights, 2013 November 6, 7, 8, with the 0.75-m APT installed at Fairborn Observatory in Arizona (Table 4), and later obtained data concurrent with the *K2* observations (see Section 4.3.2). Observations were scheduled and taken remotely and consist of 20-s integrations through a Johnson *B* filter with a photometric aperture of 30 arcsec. No comparison stars were observed as the pulsation period is known and the fluctuations in the sky transparency occur at frequencies much lower than the pulsation and therefore do not interfere. Disregarding comparison stars enabled us to maximize our time on target and provide continuous observations per night.

The data were reduced and corrected for the dead time of the detector, the sky values were fitted and subtracted from the target and the extinction corrected for using Bouguer's law and a standard site extinction coefficient of 0.24 mag/airmass for the *B* filter. Finally, the data times were adjusted to BJD.

Before analysing the pulsation in the APT data, we pre-whitened the light curves individually to a level of 0.6 mmag to a frequency of 24 d^{-1} with the aim of removing any remaining atmospheric effects not accounted for in the airmass correction and sky subtraction performed. As the pulsation frequency is significantly higher than this limit, this low-frequency filtering has no detrimental effect on our analysis.

The periodograms for each night of data presented in Fig. 6 show a clear increase in pulsation amplitude over the three nights that the target was observed. This is expected from the oblique pulsator model (Kurtz 1982; Bigot & Kurtz 2011), and is also observed in the *K2* observations (see Section 4.2). As the pulsation axis is often misaligned with the rotation axis in the roAp stars, the pulsation is

Table 4. Details of the APT observations, and the results of a non-linear least-squares fitting of the frequency and its harmonic. BJD is given as BJD−2450000.0, the rotation phase is calculated as in equation (1), and the zero-point of the phases is the mid-point of the individual data sets. Note the increase in amplitude of ν_1 over the three nights.

Date (UT)	BJD start	Rotation phase	Length (h)	Number of points	Label	Frequency (d^{-1})	Amplitude (mmag)	Phase (rad)
2013-11-06	6602.8108	0.873	2.95	416	ν_1	224.04±0.22	3.52±0.17	1.586 ± 0.050
					$2\nu_1$	448.06±0.64	1.21±0.17	2.847 ± 0.144
2013-11-07	6603.8021	0.907	3.02	416	ν_1	224.34±0.13	4.79±0.15	−0.266 ± 0.031
					$2\nu_1$	448.19±0.54	1.19±0.15	−0.629 ± 0.126
2013-11-08	6604.8011	0.943	3.08	416	ν_1	224.41±0.11	5.84±0.16	2.290 ± 0.026
					$2\nu_1$	448.40±0.41	1.64±0.16	−1.797 ± 0.095

Downloaded from http://mnras.oxfordjournals.org/ at Keele University on August 15, 2016

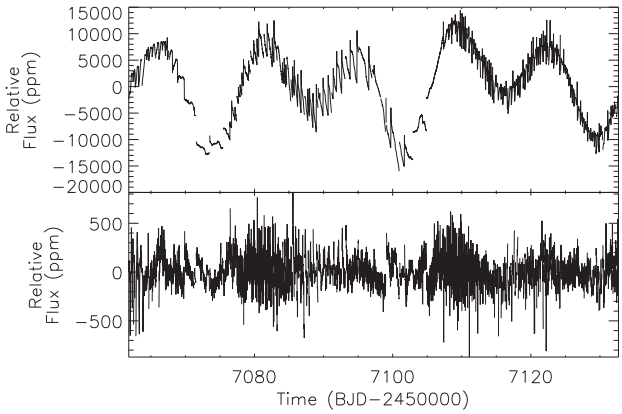

Figure 7. A comparison of the raw *K2* long cadence light curve (top) for HD 24355 and the K2P^2 pipeline light curve (bottom). Clearly, the low-frequency thruster firings are removed by the K2P^2, but so is the astrophysical signal of rotation. This is not surprising, since the K2P^2 pipeline was not designed to handle reduction of rotational variations on the time-scale seen in HD 24355. Note the extreme change in ordinate scale between the two panels.

viewed from varying aspects over the rotation period, giving rise to the amplitude variations we see in HD 24355.

Also evident in the periodograms is the presence of the first harmonic of the principal pulsation (cf. Fig. 6 and Table 4). This is often seen in roAp stars.

The amplitude of the pulsation increases over the three nights of observations (Table 4). Calculating the rotation phase at which the observations occur, using equation (1), we are able to show that they were obtained as the star was approaching maximum light in its rotation cycle, and maximum pulsation amplitude (see Section 4.3). The observations of increasing pulsation amplitude are therefore an expected outcome, as predicted by the oblique pulsator model.

4.2 *K2* observations

HD 24355 was observed as part of Campaign 4 (proposal number GO4014) of the *K2* mission. The observations covered a period of 70.90 d. There are now available many community reduction pipelines in operation for *K2* data, each resulting in slightly different light curves. This is particularly evident when dealing with the low-frequency rotational modulation which is seen in HD 24355. The data reduction performed by the K2P^2 pipeline of Lund et al. (2015) and Handberg & Lund (2014) removes the low-frequency rotational variability as the code uses a running moving-median filter to remove the spacecraft thruster firings. Fig. 7 shows a comparison between the raw *K2* light curve and the K2P^2 light curve where clearly the rotational low frequencies are removed. Currently, only long cadence data reduced with K2P^2 are available for HD 24355. Therefore, rather than using a community provided reduction pipeline, we reduced the data manually using the PYKE tools provided by the *K2* Guest Observer Office (Still & Barclay 2012).

4.2.1 *Data reduction*

The raw light curve was reduced with the PYKE tools. A pixel mask was chosen using the KEPMASK tool, and is shown in Fig. 8. Care was taken to avoid the fainter object to the lower left of the target. This star, V478 Tau, is located 18.8 arcsec from HD 24355 and is a known $B = 15.0$ flare star classified M3-M4 by Parsamyan & Oganyan (1993). We also note that the proper motion of V478 Tau

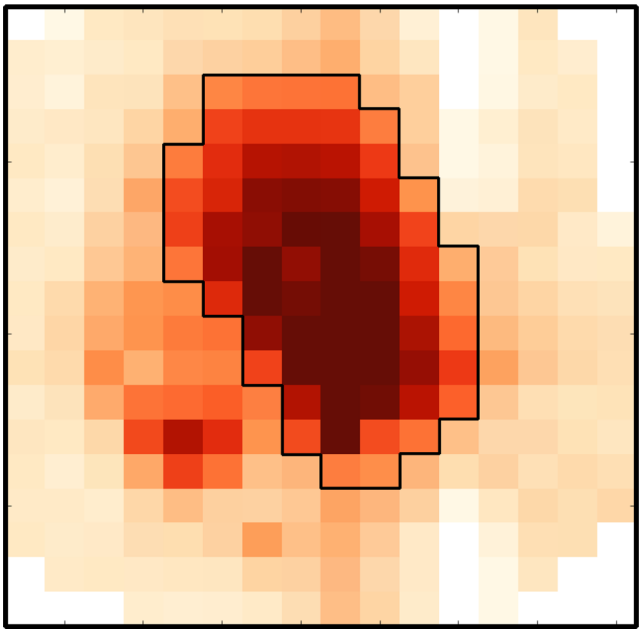

Figure 8. The pixel mask for HD 24355. The entire area is that downloaded from the spacecraft, with the solid line being the mask used to extract the light curve in this work. Note the presence of V478 Tau in the lower left. The mask was chosen to minimize light from this source.

differs from that of HD 24355 indicating that the two stars are not physically associated.

The light curve was extracted using KEPEXTRACT, which included a background subtraction, and then cleaned of obvious spurious points, resulting in 102 917 data points with which we conducted the analysis. We did not attempt to remove the motion systematics from the data with the PYKE tools; in an attempt to do so, low-frequency stellar variability was also removed, just as with the K2P^2 pipeline. Due to the high amplitude of the rotation signature, we are still able to reliably extract the rotation period, despite the thruster artefacts. Further to this, the low-frequency systematics are far removed from the pulsation signal, so do not interfere with the pulsation analysis. The final light curve is shown in the top panel of Fig. 9.

4.2.2 *Rotation signature*

Despite the thruster firings still being present in the data, the rotation signature is clearly seen in Fig. 9. The double-wave nature of the light curve suggests that we see both magnetic poles of the star, where the chemically peculiar spots form. The *K2* data allow us to unambiguously determine the rotation period of the star due to the highly stable nature of the spots coupled with the high photometric precision.

Using PERIOD04 we calculate an amplitude spectrum to 0.5 d^{-1}. The result shows two peaks, corresponding to the two consecutive dimmings in the light curve (Fig. 10). The principal peak is found at a frequency of $0.071\,642 \pm 0.000\,011$ d^{-1}, with the secondary at $0.036\,121 \pm 0.000\,019$ d^{-1}, as seen in the WASP data. The errors presented here are the analytical errors calculated using PERIOD04 following the method of Montgomery & O'Donoghue (1999). When phasing the data on the principal peak, it is clear that this is not the correct frequency which describes the modulation of the light curve, rather the lower amplitude peak provides a 'clean' phased light curve (when ignoring the spacecraft motion). Fig. 10 shows the light curve phased on the lower frequency. This is clearly the

Downloaded from http://mnras.oxfordjournals.org/ at Keele University on August 15, 2016

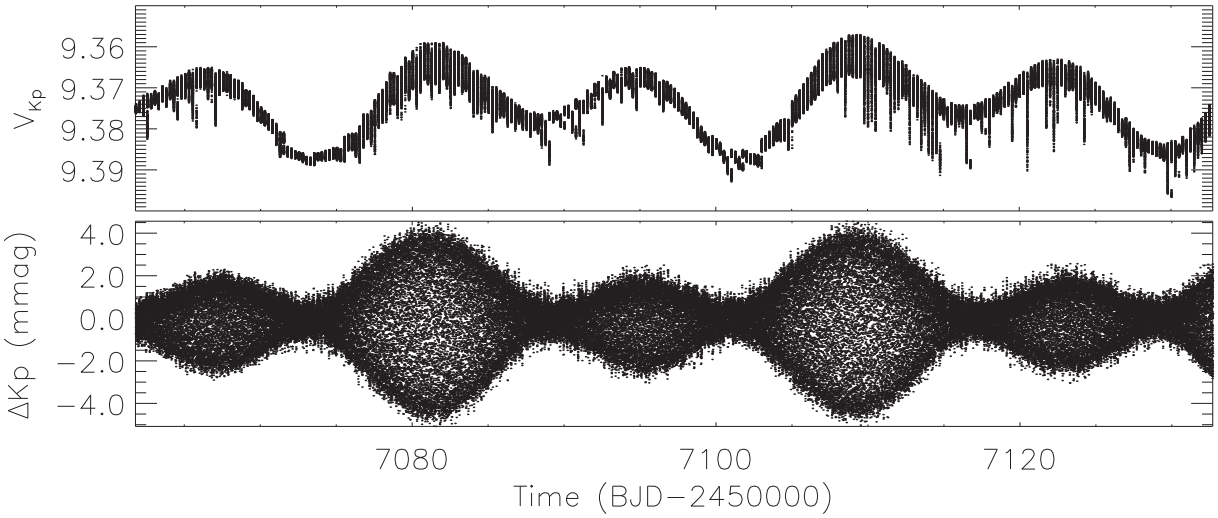

Figure 9. Top: full *K2* light curve after data reduction and cleaning has been performed. Clearly evident is the rotational signal, as well as the spacecraft motions which have not been removed. Bottom: light curve of HD 24355 after removal of the rotation signature, and cleaning of low-frequency peaks from the periodogram; these include the harmonics of the thruster frequency. The pulsation envelope is evident, with pulsational maximum occurring at the same time as rotation light maximum within the errors.

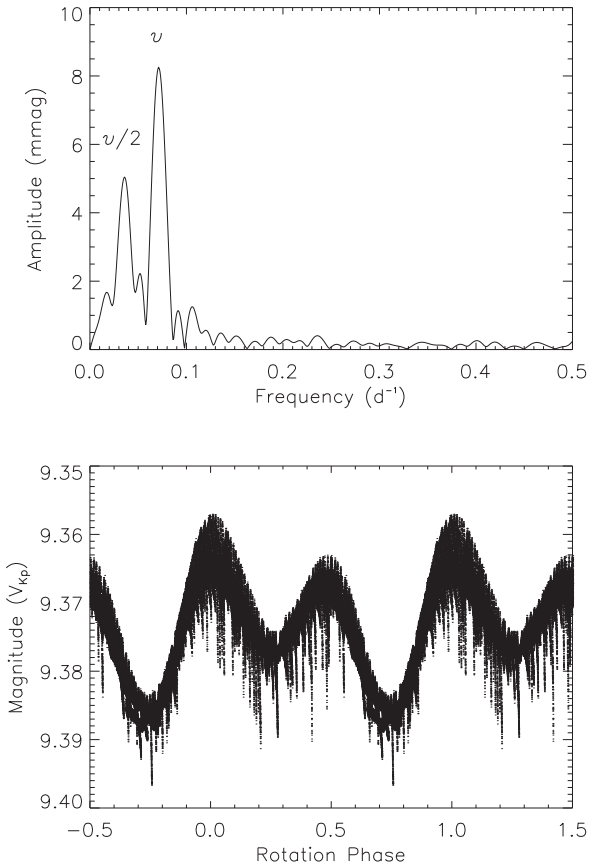

Figure 10. Top: periodogram of the *K2* light curve, showing the strongest peak at ν, as seen in WASP, and a sub-harmonic at $\nu/2$. Bottom: *K2* phased light curve, phased on a period of 27.9166 d, corresponding to the lower amplitude peak in the top panel. The phases have been calculated according to equation (1).

correct rotation frequency. This then provides us with a model of a double-wave spot variation, and the knowledge that the two peaks in Fig. 10 are harmonics. Taking the highest amplitude harmonic, i.e. the peak at 0.071 642 d^{-1}, and dividing by two provides us with an accurate rotation frequency. We use the highest amplitude harmonic as its frequency can be determined to a higher precision. In following this procedure, we determine a rotation period of the star to be 27.9166 ± 0.0043 d. This exercise has allowed us to determine the correct rotation frequency of HD 24355, and remove the ambiguity seen in the WASP data. Due to the relatively short length of the K2 data (covering ∼2.5 rotation periods), we take the period derived from the WASP data (which covers ∼57.3 rotation periods) as the rotation period for HD 24355, namely $P = 27.9158 \pm 0.0025$ d.

This result removes the ambiguity between the signals derived from the WASP data above. Due to the noise characteristics of the WASP data, especially at low frequencies, it was not possible to identify the correct rotation period from the light curve. We use the period derived from the *K2* data throughout this work.

4.2.3 Pulsation signature

Clearly evident in the *K2* periodogram of HD 24355 is the pulsation detected by both the WASP and APT observations. To study the pulsation in detail, we remove the rotation signature from the light curve and significant peaks in the low-frequency domain. This process results in the light curve shown in the bottom panel of Fig. 9. This cleaned light curve consists of 101 427 points. Fig. 11 shows a periodogram of the reduced and cleaned data set. Due to the irregularities of the thruster corrections, there remain some artefacts in the periodogram which we have not removed. The highest amplitude example of one of these artefacts occurs at about 84.5 d^{-1} with an amplitude of just 0.041 mmag. The presence of these low-amplitude peaks does not affect our analysis.

Fig. 12 shows the pulsation at a frequency of 224.3043 d^{-1} at an amplitude of 1.74 mmag, and four of the sidelobes of the principal peak after it has been removed. The pulsation is similar to that seen in the WASP data (Fig. 5), where there is a quintuplet split by the

Downloaded from http://mnras.oxfordjournals.org/ at Keele University on August 15, 2016

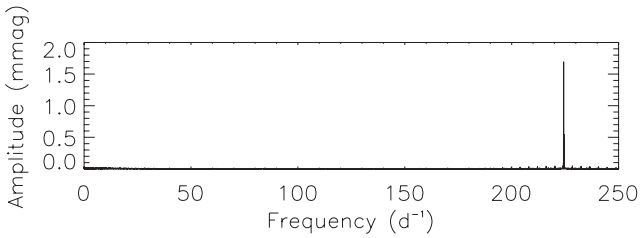

Figure 11. Periodogram of the reduced and cleaned *K2* light curve. Clearly evident is the pulsation at 224.3 d^{-1} and its window pattern generated by the ∼6-h thruster firings. There is still some low-frequency noise remaining in the data.

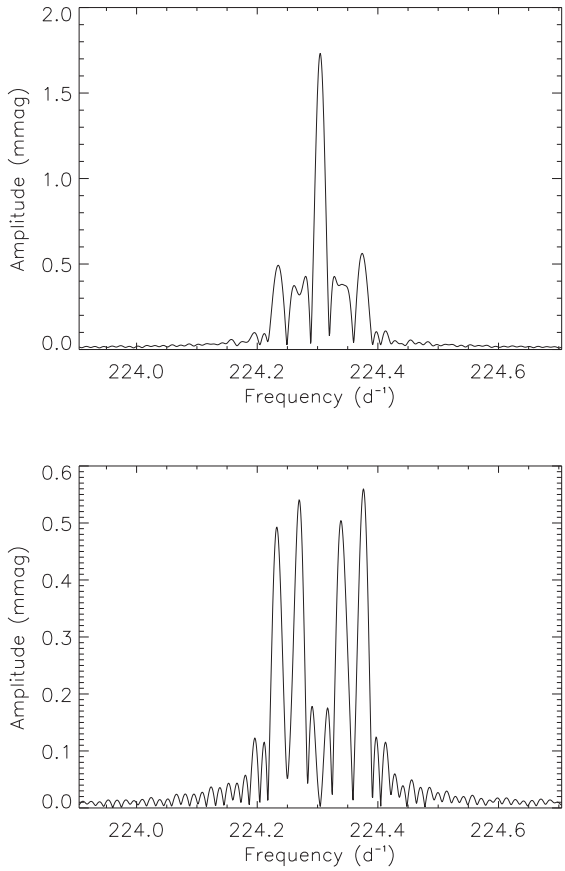

Figure 12. Top: the pulsation signature in the *K2* SC data which shows a quintuplet separated by the rotation frequency. Bottom: the rotational sidelobes after the central peak, which is the actual pulsation frequency, has been removed. Analysis of the sidelobe amplitudes informs us on the geometry of the star (see the text). Note the amplitude change between the two panels.

rotation period. Removing the four peaks shown in Fig. 12 reveals further power at frequencies split by ever increasing multiples of the rotation frequency. In total, we identify 13 rotational sidelobes ($\nu + 7\nu_{\rm rot}$ is below the noise level), the most ever seen in a roAp star. Fig. 13 demonstrates the pre-whitening of the sidelobes in the *K2* data.

The results of a non-linear least-squares fit to the data are shown in Table 5. The frequency difference, calculated in the final column of that table, shows how closely the frequency splitting matches the rotation frequency of the star, as derived from the spots. Within the calculated errors, all sidelobes are in agreement (disregarding the peak at $\nu + 8\nu_{\rm rot}$ due to the lack of a peak at $\nu + 7\nu_{\rm rot}$). This shows that the oblique pulsation model is a good match to the observations of HD 24355.

The oblique pulsation model expects that the frequencies of the sidelobes are exactly split by the rotation frequency. Therefore, using the rotation period derived from the spot variations, we force the frequencies to be equally split, and perform a linear least-squares fit to the data. When performing this test, we set the zero-point in time such that the phases of the first sidelobes are equal. The results of this test are shown in Table 6. When the exact splitting of the sidelobes is set, we see that the phases of the central five peaks are similar. For a pure quadrupole mode, we expect a quintuplet of frequencies with all phases equal at the time of pulsation maximum. Since this is not the case here for the phases of the quintuplet frequencies, and because there are further rotational sidelobes, we conclude that the mode is distorted.

4.3 Frequency variability and a rotational view of the pulsation geometry

Many of the roAp stars that have been observed at such a high photometric precision as that afforded by the *Kepler* spacecraft have shown significant variations in their pulsation frequencies over the observation period (e.g. Holdsworth et al. 2014b; Smalley et al. 2015). To this end, we investigate this phenomenon in HD 24355. We split the data into sections of 100 pulsation cycles, or about 0.45 d. This provides us with a suitable number of data points per section with which to calculate a periodogram over, and ample time resolution to detect any frequency variability. For this exercise, we use the data that have had the rotation signature, and its harmonics, removed (Fig. 9, bottom).

By calculating the frequencies, amplitudes and phases of the pulsation in these sections of data, we are able to monitor the variations of the pulsation over the rotation period of the star. Fig. 14 shows the variation of the pulsation amplitude over the rotation period of the star. As is expected from the oblique pulsator model, the amplitude varies over the rotation cycle, as the pulsation mode is seen from varying aspects. The maximum amplitude coincides with light maximum which is expected when the spots producing the light variations are closely aligned with the magnetic and pulsation poles. The amplitude does not reach zero. If the mode were a pure mode, the amplitude would go to zero whenever the line of sight passes over a pulsation node; as this is not the case here, we can see that the mode is distorted. Other than the expected rotational amplitude variation, the pulsational amplitude is stable over the ∼2.5 rotations that the observations cover.

The phase variations seen in Fig. 14 are very different from those seen in other roAp stars (e.g. see fig. 10 of Kurtz et al. 2011). When the line of sight passes over a node, the oblique pulsator model predicts a π-rad phase shift for a pure dipole or quadrupole mode. This is not the case here, thus supporting the conclusion that HD 24355 is a distorted pulsator.

To compare this star with others which show distorted dipole pulsations, we have performed the same analysis on HR 3831, HD 6532, HD 99563 and KIC 10195926 (Kurtz et al. 1996, 1997, 2011; Handler et al. 2006). All of these stars, as well as HD 24355, show a double-wave rotationally modulated light curve, and phase changes at minimum light. Fig. 15 shows this comparison. While the other stars show a clear phase change of about π rad at quadrature, the phase variations seen in HD 24355 are dramatically different. Such an unusually small change in phase,

Downloaded from http://mnras.oxfordjournals.org/ at Keele University on August 15, 2016

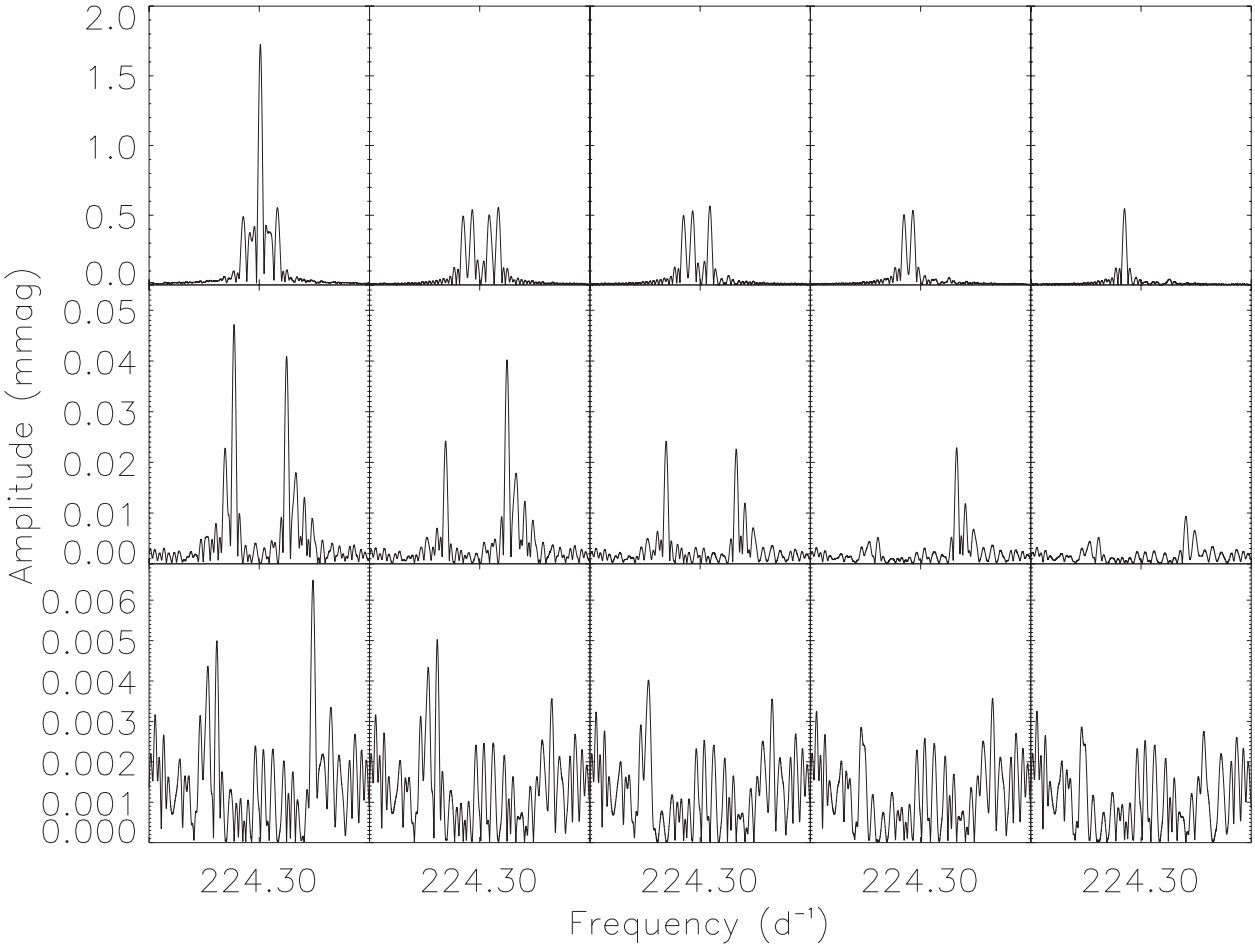

Figure 13. The pre-whitening of the pulsation and its sidelobes in the *K2* data. The panels are read left to right, top to bottom. Note the change in amplitude scale on the different rows.

Table 5. The results of a non-linear least-squares fit to the *K2* light curve. The last column shows the difference in the frequency between that line and the previous. The zero-point for the phases is BJD−2457097.2393.

ID	Frequency (d^{-1})	Amplitude (mmag)	Phase (rad)	Frequency difference (d^{-1})
$\nu - 6\nu_{rot}$	224.089 25 ± 0.003 49	0.004 ± 0.002	0.346 ± 0.444	
$\nu - 5\nu_{rot}$	224.126 96 ± 0.002 89	0.005 ± 0.002	−0.828 ± 0.367	0.037 71 ± 0.004 53
$\nu - 4\nu_{rot}$	224.160 98 ± 0.000 59	0.025 ± 0.002	−2.237 ± 0.075	0.034 02 ± 0.002 95
$\nu - 3\nu_{rot}$	224.197 13 ± 0.000 32	0.049 ± 0.002	2.051 ± 0.038	0.036 15 ± 0.000 67
$\nu - 2\nu_{rot}$	224.232 65 ± 0.000 03	0.553 ± 0.002	2.116 ± 0.003	0.035 52 ± 0.000 32
$\nu - 1\nu_{rot}$	224.268 46 ± 0.000 03	0.596 ± 0.002	−0.299 ± 0.003	0.035 81 ± 0.000 04
ν	224.304 30 ± 0.000 01	1.863 ± 0.002	3.080 ± 0.001	0.035 84 ± 0.000 03
$\nu + 1\nu_{rot}$	224.340 11 ± 0.000 03	0.599 ± 0.002	0.741 ± 0.003	0.035 81 ± 0.000 03
$\nu + 2\nu_{rot}$	224.375 97 ± 0.000 03	0.627 ± 0.002	−2.264 ± 0.003	0.035 86 ± 0.000 04
$\nu + 3\nu_{rot}$	224.411 45 ± 0.000 37	0.044 ± 0.002	−1.599 ± 0.042	0.035 48 ± 0.000 37
$\nu + 4\nu_{rot}$	224.447 17 ± 0.000 71	0.023 ± 0.002	1.806 ± 0.082	0.035 72 ± 0.000 80
$\nu + 5\nu_{rot}$	224.483 30 ± 0.001 54	0.010 ± 0.002	2.562 ± 0.191	0.036 13 ± 0.001 70
$\nu + 6\nu_{rot}$	224.518 95 ± 0.002 11	0.007 ± 0.002	0.815 ± 0.268	0.035 65 ± 0.002 61
$\nu + 8\nu_{rot}$	224.593 82 ± 0.003 95	0.004 ± 0.002	0.833 ± 0.499	0.074 87 ± 0.004 48

and the number of sidelobes identified in the pulsation, shows that the star has the most distorted pulsation mode of any roAp star yet observed.

Beyond the known pulsation in HD 24355, no further modes were identified in the *K2* data.

4.3.1 Mode geometry constraints

As the *K2* data have a much higher precision than ground-based data, we can derive parameters of the geometry of the pulsation mode using the ratios of the sidelobes following the methodology of Kurtz, Shibahashi & Goode (1990). Initially, we test the phase relations

Downloaded from http://mnras.oxfordjournals.org/ at Keele University on August 15, 2016

Table 6. The results of a linear least-squares fit to the *K2* light curve. The zero-point has been chosen to be BJD 2457108.886701 to force the phases of the first rotational sidelobes to be equal.

ID	Frequency (d^{-1})	Amplitude (mmag)	Phase (rad)
$\nu - 6\nu_{rot}$	224.089 368	0.004 ± 0.002	0.782 ± 0.445
$\nu - 5\nu_{rot}$	224.125 190	0.005 ± 0.002	2.180 ± 0.367
$\nu - 4\nu_{rot}$	224.161 012	0.025 ± 0.002	−2.850 ± 0.074
$\nu - 3\nu_{rot}$	224.196 834	0.049 ± 0.002	−2.225 ± 0.037
$\nu - 2\nu_{rot}$	224.232 656	0.553 ± 0.002	0.465 ± 0.003
$\nu - 1\nu_{rot}$	224.268 478	0.596 ± 0.002	0.672 ± 0.003
ν	224.304 300	1.863 ± 0.002	0.388 ± 0.001
$\nu + 1\nu_{rot}$	224.340 122	0.598 ± 0.002	0.671 ± 0.003
$\nu + 2\nu_{rot}$	224.375 944	0.627 ± 0.002	0.288 ± 0.003
$\nu + 3\nu_{rot}$	224.411 766	0.044 ± 0.002	−2.710 ± 0.042
$\nu + 4\nu_{rot}$	224.447 588	0.023 ± 0.002	−2.966 ± 0.081
$\nu + 5\nu_{rot}$	224.483 410	0.010 ± 0.002	0.397 ± 0.188
$\nu + 6\nu_{rot}$	224.519 232	0.007 ± 0.002	1.267 ± 0.272

between the pulsation mode and the first rotational sidelobes by forcing the sidelobes to have the same phase. We find that $\phi_{-1} = \phi_{+1} \neq \phi_0$, suggesting that the mode is distorted (Table 6).

The clear frequency quintuplet strongly suggests that the pulsation is quadrupolar. We therefore examine the axisymmetric quadrupole case, where $l = 2$ and $m = 0$, applying a relationship from Kurtz et al. (1990) for a non-distorted oblique quadrupole pulsator in the absence of limb darkening and spots, i.e.

$$\tan i \tan \beta = 4 \frac{A^{(2)}_{+2} + A^{(2)}_{-2}}{A^{(2)}_{+1} + A^{(2)}_{-1}}, \quad (2)$$

where i is the rotational inclination angle, β is the angle of obliquity between the rotation and magnetic axes, and $A^{(2)}_{\pm 1}$ and $A^{(2)}_{\pm 2}$ are the amplitudes of the first and second sidelobes of the quadrupole pulsation, respectively. Using the amplitudes from Table 6 again, and substituting them into equation (2), we derive $\tan i \tan \beta = 3.950 \pm 0.012$ for this simplified case.

Table 7 shows a set of values of i and β that satisfy the constraint of equation (2). All possible values sum to greater than 90°, which is consistent with the rotational light modulation under the assumption that there are spots at both magnetic/pulsation poles. Values of i and β near to 90° are not permitted for a quadrupole mode, within the constraint of equation (2), because the line of sight would then not pass over a node. However, we have a stronger constraint on the inclination: from our spectra we are able to place an upper limit of $v \sin i \leq 3.5$ km s^{-1}. Using this value, the rotation period of 27.9158 d and the derived radius of $R = 2.53\,R_\odot$, we can estimate an upper limit of $i \leq 50°$.

Using these values for i and β, we apply the method of Kurtz (1992), based on work by Shibahashi & Takata (1993), to deconvolve the pulsation into the components of a spherical harmonic series. This technique separates the distorted mode into its pure $\ell = 0, 1, 2, \ldots$ spherical harmonic components, allowing us to see the shape of the mode. The results of this deconvolution are shown in Tables 8 and 9. The results show that the mode is a quadrupole mode with a strong spherically symmetric distortion represented by the radial component. The $\ell = 1$ and 3 components are small in comparison.

Similarly to the APT data, the *K2* data show harmonics of the pulsation. These harmonics are present up to and including the 4th, i.e. $5\nu = 1121.5215$ d^{-1}, where at higher frequencies any signal is lost in the noise. This demonstrates the non-sinusoidal nature of pulsations in roAp stars.

The opportunity to observe a high-amplitude, classically ground-based, roAp star with *K2* precision provided, for the first time, the chance to compare the space- and ground-based targets. It is unclear, due to the detection limits from the ground, and the small sample of stars observed at μmag precision, whether there is a fundamental difference between the high-amplitude ground-based targets and the low-amplitude space-based targets. The observations presented here, although for only one of the 57 ground-based targets, suggest that there may be an 'amplitude desert' in the roAp stars. However, many more observations of ground-based roAp stars at μmag precision are needed to test whether there really is such a dichotomy.

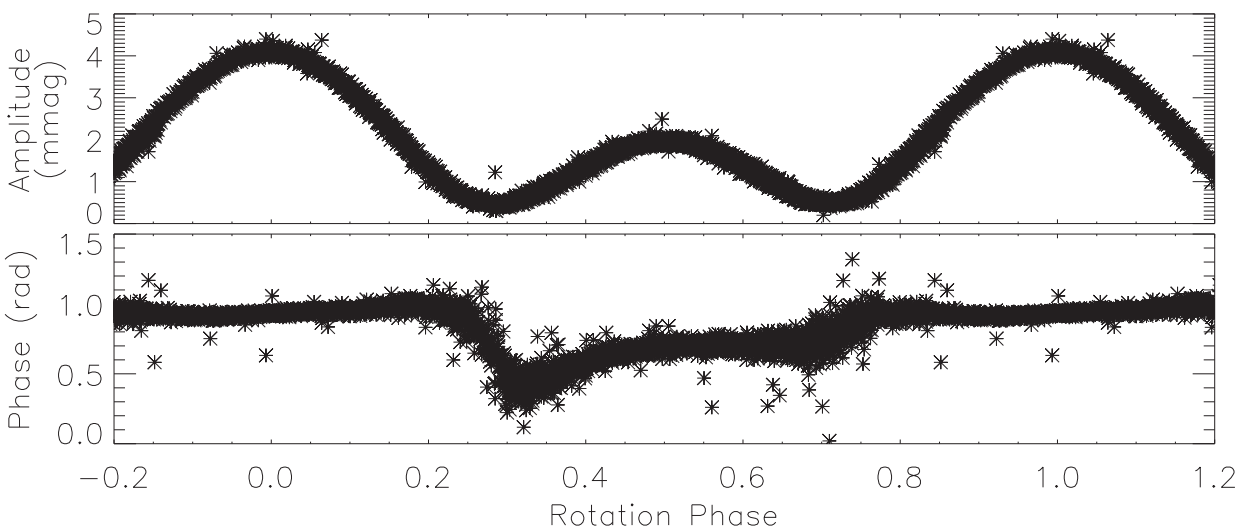

Figure 14. Top: the variation of the pulsation amplitude as a function of rotation phase. This shows that the pulsation amplitude coincides with the rotational light extremum. The double-wave nature of the light curve is indicative of a pulsation mode seen from varying aspect where the line of sight crosses one pulsation node. In this case, the mode is a quadrupole. Bottom: the pulsation phase variation as a function of rotation phase. There is a phase change as the line of sight passes over pulsation nodes; however, such a small change is indicative of an extremely distorted mode. The rotation phases are calculated as in equation (1).

Downloaded from http://mnras.oxfordjournals.org/ at Keele University on August 15, 2016

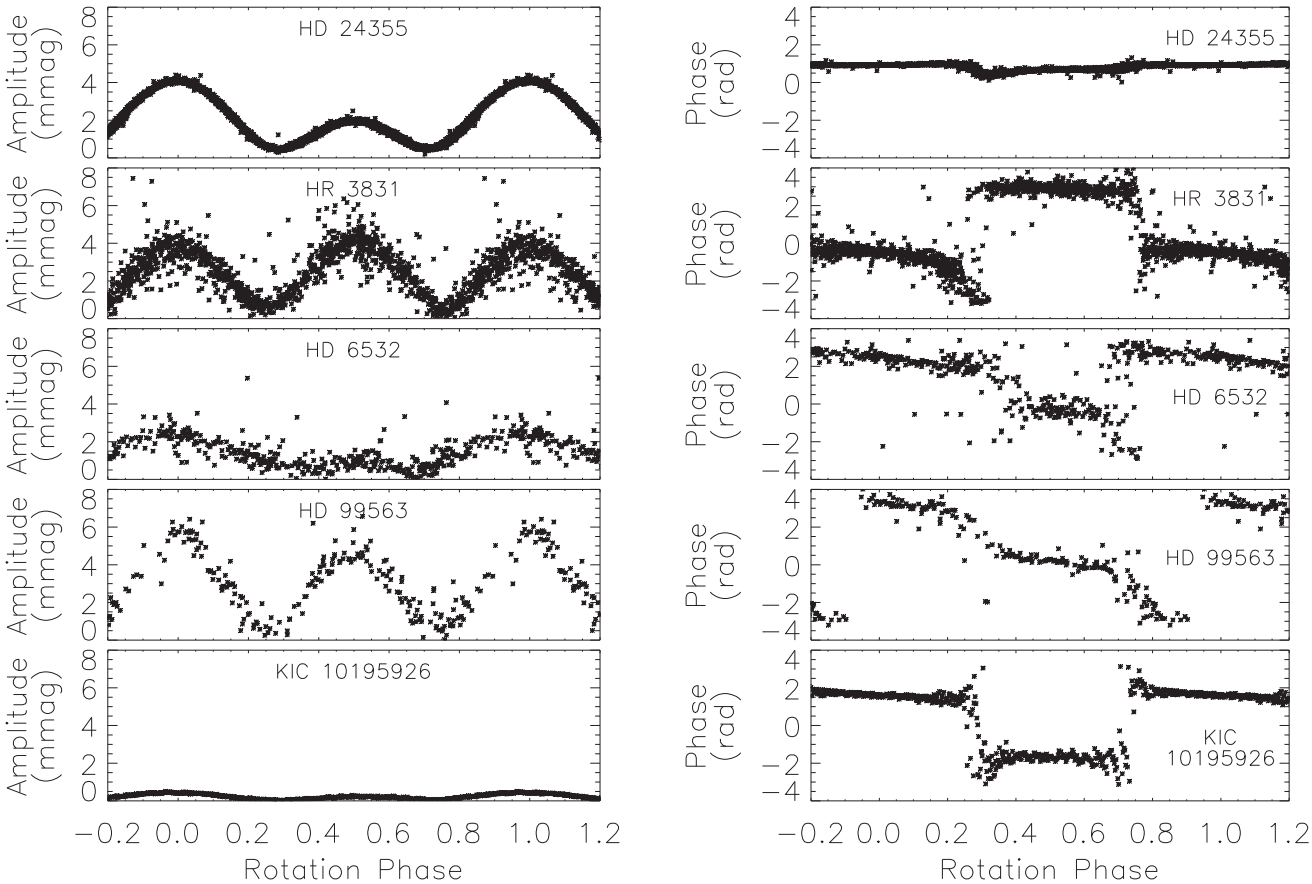

Figure 15. Pulsation amplitude and phase variations as a function of rotation phase for a set of roAp stars which are distorted dipole pulsators. All plots are on the same scale for easy comparison, and have been calculated in the same way. The stars are labelled in the plots. Despite all being distorted dipoles, there is a clear difference between the previously studied stars and HD 24355. Note that the phases are different from those previously published for the comparison stars as a different zero-point was chosen.

Table 7. Values of i and β which satisfy equation (2). We list values up to $i = \beta$, where the values of i and β are reversed. The columns $i - \beta$ and $i + \beta$ show the extreme values of the angle between the line of sight and the pulsation pole; these can be useful in visualizing the pulsation geometry.

i	β	$i - \beta$	$i + \beta$
89.0	3.9	85.1	92.9
85.0	19.0	66.0	104.0
80.0	34.9	45.1	114.9
75.0	46.6	28.4	121.6
70.0	55.2	14.8	125.2
65.0	61.5	3.5	126.5
63.1	63.1	0.0	126.2

Table 8. Components of the spherical harmonic series description of the pulsation for $i = 45°$ and $\beta = 77°$.

ℓ	0	1	2	3
$A_{-3}^{(\ell)}$ (mmag)				0.049
$A_{-2}^{(\ell)}$ (mmag)			0.623	0.066
$A_{-1}^{(\ell)}$ (mmag)		0.123	0.629	−0.067
$A_{0}^{(\ell)}$ (mmag)	2.353	0.063	−0.416	0.025
$A_{+1}^{(\ell)}$ (mmag)		0.148	0.661	−0.064
$A_{+2}^{(\ell)}$ (mmag)			0.678	0.062
$A_{+3}^{(\ell)}$ (mmag)				0.044
ϕ (rad)	0.007	2.664	0.114	−2.621

4.3.2 Comparison of K2 and APT data

The availability of both the broad-band *K2* observations and the three nights of *B*-band APT data allows us to directly compare the amplitudes of the different data sets, and estimate the maximum pulsation amplitude of HD 24355 in a *B*-band filter. From Table 4, we know the rotation phase at which the APT data were obtained, namely at phases 0.873, 0.907 and 0.943. We compare the amplitudes of the APT data at these phases to the amplitudes of the *K2* data at the same phases in Table 10. We can see that the amplitude ratio is increasing with time, so rather than take an average of the

Table 9. Comparison between the observed amplitudes and phases to those calculated with the spherical harmonic fit.

ID	$A_{\rm obs}$	$A_{\rm calc}$	$\phi_{\rm obs}$	$\phi_{\rm calc}$
$\nu - 3\nu_{\rm rot}$	0.049 ± 0.002	0.049	-2.621 ± 0.038	−2.621
$\nu - 2\nu_{\rm rot}$	0.553 ± 0.002	0.553	0.067 ± 0.003	0.067
$\nu - 1\nu_{\rm rot}$	0.596 ± 0.002	0.596	0.275 ± 0.003	0.275
ν	1.863 ± 0.002	1.863	-0.008 ± 0.001	−0.008
$\nu + 1\nu_{\rm rot}$	0.598 ± 0.002	0.603	0.275 ± 0.003	0.288
$\nu + 2\nu_{\rm rot}$	0.627 ± 0.002	0.621	-0.108 ± 0.003	−0.076
$\nu + 3\nu_{\rm rot}$	0.044 ± 0.002	0.044	-3.107 ± 0.042	−2.621

Downloaded from http://mnras.oxfordjournals.org/ at Keele University on August 15, 2016

Table 10. Comparison of the APT *B*-band observations from 2013 November and *K2* pulsation amplitudes at given rotation phases.

Rotation Phase	$A_{\rm APT}$ (mmag)	$A_{\rm K2}$ (mmag)	$A_{\rm APT}/A_{\rm K2}$
0.873	3.52 ± 0.17	2.63 ± 0.13	1.34 ± 0.09
0.907	4.79 ± 0.15	3.25 ± 0.06	1.47 ± 0.05
0.943	5.84 ± 0.16	3.64 ± 0.05	1.60 ± 0.05

Table 11. APT multi-colour photometry of HD 24355, taken at rotation phase 0.400.

Filter	Amplitude (mmag)	$A_{\rm APT}/A_{\rm K2}$
U	3.02 ± 0.78	2.54 ± 0.66
B	5.17 ± 0.51	4.34 ± 0.47
V	1.67 ± 0.48	1.40 ± 0.41
K2	1.19 ± 0.05	

ratio, we use a linear extrapolation to the maximum of the pulsation in the *K2* data, which is measured to be $A_{\rm K2} = 4.10 \pm 0.09$. This gives us a maximum *B*-band amplitude of 6.90 ± 1.93 mmag. Comparing this amplitude with other roAp stars in the literature for which *B*-band amplitudes are known (e.g. Kurtz et al. 2006; Holdsworth 2015), this is not a surprising result for HD 24355.

Further to the three nights of observations in 2013 November, we observed HD 24355 with the APT simultaneously with *K2*. These coincident observations were made in three filters, *U*, *B* and *V*. Observations were taken as in 2013 but cycling through each of the three filters sequentially. We attempted to observe the star throughout the *K2* observations; however, due to the poor visibility of the target, from Earth, during the *K2* campaign we were unable to obtain long periods on target, recording only 665 data points per filter over a 26-d period. These multi-colour data are still useful. We combine the two best nights of data, namely BJD 2457091.6 and 2457092.6, and fit the pulsation by non-linear least-squares. The results of the fitting are presented in Table 11. To compare the multi-colour data to *K2* observations, we extract the same time period from the *K2* data and compute the pulsation amplitude in the same way. Again, it is clear that the amplitude seen in the white light *Kepler* filter is greatly reduced when considering the *B*, or even *U*, band observations, an expected result from multi-colour photometric studies (Medupe & Kurtz 1998).

We observe here that the *B*-band amplitude at $\phi_{\rm rot} = 0.400$ is greater than the *K2* amplitude by a factor of 4.34 ± 0.47. This is a much greater ratio than the observations at $\phi_{\rm rot} = 0.943$, close to maximum pulsation amplitude. For the values of i and β which produce the best model to the data (see Section 5), namely $i = 45^\circ$ and $\beta = 77^\circ$, we see the pulsation poles at 32° and 58° to the line of sight, corresponding to the pulsation primary and secondary maxima, respectively. We postulate, therefore, that the variation in the amplitude ratio between *B*-band and *K2* observations is a result of a different line of sight to the pulsation pole, and as such we are probing higher in the atmosphere where pulsation amplitudes are greater for certain spectral lines (e.g. Kurtz 2006), and possibly in broad-band photometry too. We would then expect the *B*-band amplitude of the secondary light maximum at $\phi_{\rm rot} = 0.5$ to be of the order of 8.65 ± 0.94 mmag, thus shifting the maximum amplitude, in the *B* band, by half a rotation period. To test the relation between pulsation amplitude, rotation phase (or light-of-sight aspect) and atmospheric depth requires multi-colour photometry covering the entire rotation period of the star.

5 MODELLING THE AMPLITUDE AND PHASE MODULATION

5.1 Equations

We assume that the rapid pulsation of HD 24355 is an axisymmetric (with respect to the magnetic axis) high-order p mode. The presence of four main rotational sidelobes' frequencies indicates the pulsation to be a quadrupole mode. However, in the presence of a magnetic field (assuming a dipole field) no pure quadrupole mode exists, because the Legendre function $P_\ell(\cos\theta_B)$ couples to another $P_{\ell'}(\cos\theta_B)$ if $\ell' = \ell \pm 2$; i.e. the magnetic field distorts the angular distribution of amplitude.

The distribution of the local luminosity perturbation on the surface may be expressed by a sum of terms proportional to $Y^0_{\ell_j}(\theta_B, \phi_B)[= N_{\ell_j 0} P_{\ell_j}(\cos\theta_B)]$ with even degrees $\ell_j = 0, 2, 4, \ldots$ as

$$\delta F(\theta_{\rm B}, \phi_{\rm B}, t) = {\rm e}^{{\rm i}\sigma t} \sum_{j=1}^{J} f_j N_{\ell_j 0} P_{\ell_j}(\cos\theta_{\rm B}), \tag{3}$$

where $\ell_j = 2(j-1)$, $N_{\ell_j 0} = \sqrt{(2\ell_j + 1)/(4\pi)}$ and $(\theta_{\rm B}, \phi_{\rm B})$ are spherical coordinates whose axis is along the magnetic axis. The luminosity perturbation at the surface for each component f_j is obtained by solving non-adiabatic non-radial pulsation equations (truncated at $j = J$) which include the effect of a dipole magnetic field (Saio 2005). In the absence of magnetic fields, $f_j = 0$ if $j \neq 2$ for quadrupole modes, while magnetic couplings make $f_j \neq 0$ for any j.

Observational light variation may be expressed as

$$\Delta L(t) \propto {\rm e}^{{\rm i}\sigma t} \sum_{j=1}^{J} f_j N_{\ell_j,0} \int_0^{2\pi} {\rm d}\phi_{\rm L} \times \int_0^{\pi/2} {\rm d}\theta_{\rm L} \sin\theta_{\rm L} (1 - \mu + \mu\cos\theta_{\rm L}) \cos\theta_{\rm L} P_{\ell_j}(\cos\theta_{\rm B}), \tag{4}$$

where μ is the limb-darkening parameter, and $(\theta_{\rm L}, \phi_{\rm L})$ is the set of spherical coordinates on the surface, whose axis ($\theta_{\rm L} = 0$) is along the observer's line of sight. Numerical integration over the visible hemisphere can be done by using the relation between $(\theta_{\rm L}, \phi_{\rm L})$ and $\cos\theta_{\rm B}$, which is obtained from spherical trigonometry (e.g. Smart 1931). The amplitude modulation occurs because the relation is time dependent [the coordinate $(\theta_{\rm L}, \phi_{\rm L})$ at a magnetic pole changes with rotational phase].

We have neglected to consider the departure from spherical symmetry, which results from the presence of a strong magnetic field, in the determination of the luminosity variation. This effect can be safely disregarded as the ratio between the temperature variation and the radius variation is of the order of 100 for high-order p modes; thus, temperature variations are much more significant than radius variations caused by the strong magnetic field.

Another way to evaluate equation (4) is to use relations of spherical harmonics associated with polar coordinates with different axes (see Unno et al. 1989; Shibahashi & Takata 1993; Saio & Gautschy 2004). The spherical harmonic $Y^0_{\ell_j}(\theta_{\rm B}, \phi_{\rm B})$ is converted to a sum of

Downloaded from http://mnras.oxfordjournals.org/ at Keele University on August 15, 2016

terms proportional to $Y_{\ell_j}^{m''}(\theta_{\rm L}, \phi_{\rm L})$ as

$$\begin{aligned} Y_{\ell_j}^{0}(\theta_{\rm B}, \phi_{\rm B}) &= \sum_{m'=-\ell_j}^{\ell_j} Y_{\ell_j}^{m'}(\theta_{\rm R}, \phi_{\rm R}) d_{m',0}^{(\ell_j)}(\beta) \\ &= \sum_{m'=-\ell_j}^{\ell_j} Y_{\ell_j}^{m'}(\theta_{\rm I}, \phi_{\rm I}) d_{m',0}^{(\ell_j)}(\beta) {\rm e}^{-{\rm i}m'\Omega t} \\ &= \sum_{m'=-\ell_j}^{\ell_j} d_{m',0}^{(\ell_j)}(\beta) {\rm e}^{-{\rm i}m'\Omega t} \sum_{m''=-\ell_j}^{\ell_j} Y_{\ell_j}^{m''}(\theta_{\rm L}, \phi_{\rm L}) d_{m'',m'}^{(\ell_j)}(i), \end{aligned} \tag{5}$$

where coordinate $(\theta_{\rm R}, \phi_{\rm R})$ is the corotating frame with the axis along the rotation axis, which is inclined to the magnetic axis by angle β. While the axis of the system $(\theta_{\rm I}, \phi_{\rm I})$ is also the rotation axis, this is an inertial system; i.e. $\theta_{\rm I} = \theta_{\rm R}$ and $\phi_{\rm I} = \phi_{\rm R} + \Omega t$. The last equality of equation (5) relates the system $(\theta_{\rm I}, \phi_{\rm I})$ to the system $(\theta_{\rm L}, \phi_{\rm L})$ whose axis is along the line of sight and inclined to the rotation axis by angle i. Substituting the last relation in equation (5), we obtain

$$\Delta L(t) \propto {\rm e}^{{\rm i}\sigma t} \sum_{j=1}^{J} f_j N_{\ell_j 0} I_{\mu\ell_j} \sum_{m'=-\ell_j}^{\ell_j} d_{m',0}^{(\ell_j)}(\beta) d_{0,m'}^{(\ell_j)}(i) {\rm e}^{-{\rm i}m'\Omega t}, \tag{6}$$

where $I_{\mu\ell_j}$ represents the latitudinal integration

$$I_{\mu\ell_j} \equiv \int_0^1 (1 - \mu + \mu z) z P_{\ell_j}(z) {\rm d}z. \tag{7}$$

In this expression, amplitude modulation is expressed by a superposition of Fourier components at frequencies of $\sigma \pm k\Omega$ with $k = 0, 1, \ldots$, corresponding to the observational data given in Table 6.

5.2 Comparison with observation

Spectroscopic parameters of HD 24355 are $(T_{\rm eff}, \log g) = (8200 \pm 200\,{\rm K}, 4.0 \pm 0.2)$. Within and around the error box, we have searched for models that have a frequency similar to 224.30 d^{-1} and reproduce the amplitude and phase modulation.

For each model, we picked a non-magnetic quadrupole mode having a frequency similar to the observed frequency 224.3 d^{-1}. Then, assuming a polar magnetic field strength, $B_{\rm p}$, of a dipole field, we obtained non-adiabatic eigenfrequency and eigenfunction using the method discussed in Saio (2005), in which the expansion was truncated at $J = 20$ (equation 3). Using the eigenfunction in equation (6), we obtain the amplitude modulation and the amplitudes of rotational sidelobes to compare with the observations. A good fit, as presented in Fig. 16, was sought by changing $B_{\rm p}$, β and i assuming the limb-darkening parameter $\mu = 0.6$ (the effect of different μ was examined by adopting $\mu = 0.4$ and 0.8 and found that qualitative properties hardly changed). Theoretical prediction depends weakly on the inclination i. This is constrained by the fact that the rotation period of HD 24355 is 27.9158 d and an upper limit of $v \sin i \leq 3.5$ km s^{-1}. As our spectroscopic observations allow us to place an upper limit of $i < 50^\circ$, we present models with $i = 45^\circ$ as a standard choice, although we can obtain similarly good models in a wide range of i.

Although the amplitude modulation of HD 24355 can be reasonably reproduced by models with parameters around the spectroscopically derived $(T_{\rm eff}, \log g)$, qualitative properties of the phase modulation systematically change along evolutionary tracks (i.e. $T_{\rm eff}$), as shown in Fig. 17; there is a point where the direction of theoretical phase change switches; the 'amplitude' of phase modulation decreases as $T_{\rm eff}$ decreases. In producing Fig. 17, we ensure

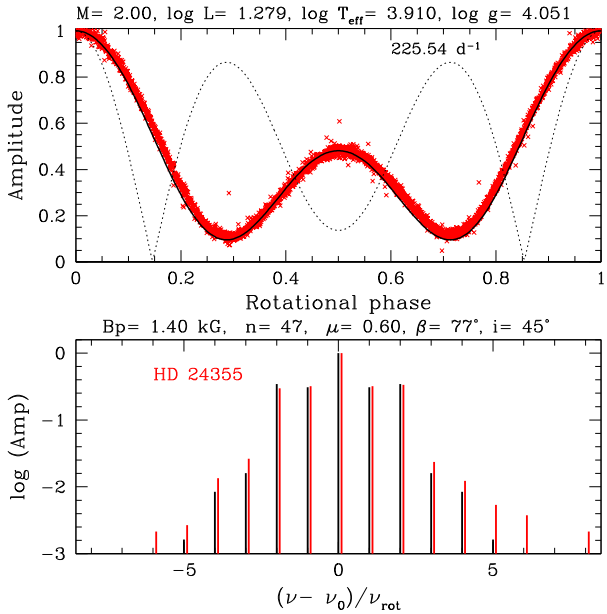

Figure 16. Amplitude modulation (top panel) and corresponding rotational sidelobes (bottom panel) of HD 24355 (red crosses and red bars) are compared with a model (black lines). The dotted line in the top panel shows amplitude modulation expected if the latitudinal distribution of pulsation were proportional to the Legendre function $P_2(\cos\theta_B)$. Note that bottom panel plots the logarithmic (base 10) values of sidelobe amplitude normalized by the amplitude of the central frequency.

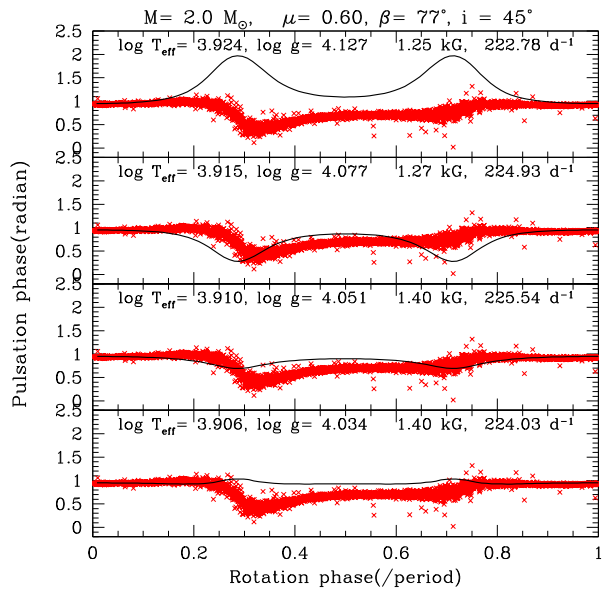

Figure 17. Pulsation phase modulation of HD 24355 (red crosses) with respect to the rotation phase is compared with theoretical ones obtained for some of the evolutionary models of 2 M$_\odot$. The effective temperature and surface gravity decrease from top to bottom.

that every model in each panel of the figure reproduces well the observed amplitude modulation, as in Fig. 16. We judge that the model in the second panel from the bottom at $\log T_{\rm eff} = 3.910$ best fits with the observed phase modulation among the 2.0 M$_\odot$ models. This model has a radius of 2.21 R$_\odot$, which gives an upper limit of $i \leq 48^\circ$ consistent with $i = 45^\circ$.

Downloaded from http://mnras.oxfordjournals.org/ at Keele University on August 15, 2016

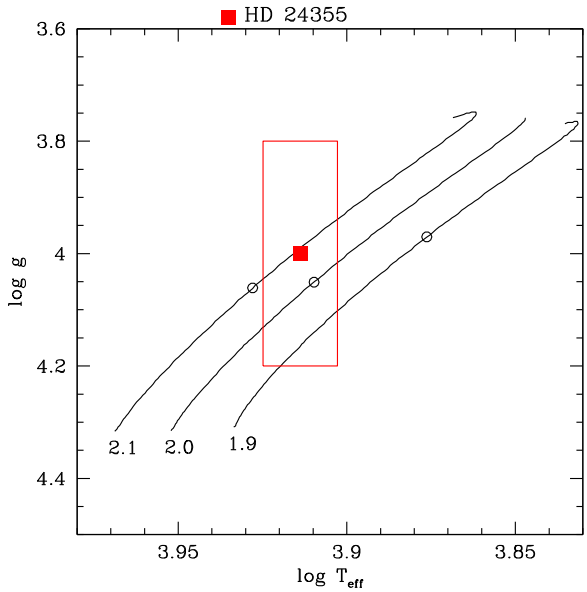

Figure 18. The log $T_{\rm eff}$–log g diagram showing the spectroscopic parameter ($T_{\rm eff}$, log g) = (8200 ± 200, 4.0 ± 0.2) of HD 24355 and evolutionary tracks of 1.9, 2.0 and 2.1 $M_{\odot}$ with a composition of (X, Z) = (0.70, 0.02). The open circle along each track indicates the model that can reproduce the amplitude and the phase modulations of HD 24355.

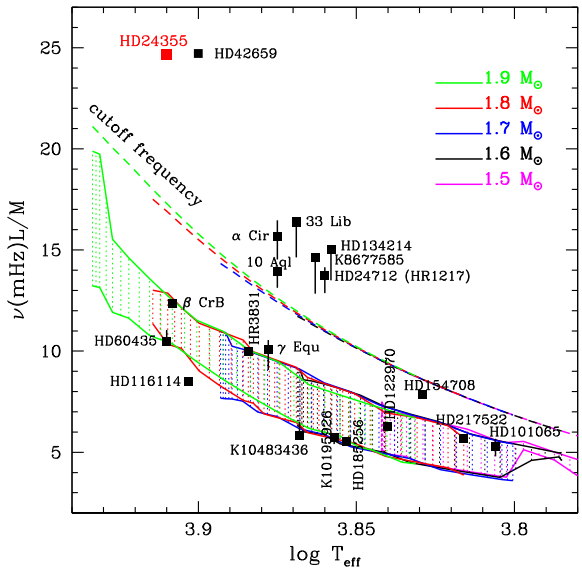

Figure 19. The position of HD 24355 in the log $T_{\rm eff}$–$\nu L/M$ plane is compared with some of the known roAp stars, in which L/M is in solar units. Main frequencies are shown by squares and frequency ranges by vertical bars. Shaded region indicates where high-order p modes are excited by the κ-mechanism in the H-ionization zone in non-magnetic models. Dashed lines show the acoustic cut-off frequencies. This figure is an extended version of fig. 3 in Saio (2014).

In this way, for each evolutionary track, we determine a model which reasonably reproduces the amplitude modulation and the phase modulation of HD 24355. The parameters of those models are shown by open circles in Fig. 18. Among the models we examined, the 2.0-$M_{\odot}$ model is consistent with the spectroscopic parameters of HD 24355. Furthermore, a relatively weak magnetic field of $B_{\rm p}$ = 1.4 kG is consistent with the absence of Zeeman splitting in the spectral lines. Such a moderate magnetic field can deform the eigenfunction significantly, because the oscillation frequency of HD 24355 corresponds to a very high order p mode whose energy is confined in superficial layers of the star.

We note that a slight asymmetry in observed phase modulation, which cannot be reproduced in our models, is probably caused by a small effect of Coriolis force (Bigot & Kurtz 2011) which we have neglected for simplicity.

Fig. 19 shows the position of HD 24355 in the log $T_{\rm eff}$–$\nu L/M$ plane together with some of the known roAp stars (details of which can be found in Table 12). In this diagram, the mass dependence of the acoustic cut-off frequency as well as the range of excitation by the κ-mechanism in the H-ionization zone (Balmforth et al. 2001) is partially compensated for. This figure shows that HD 24355 is a peculiar roAp star whose pulsation is highly supercritical – much more so than for the stars in the well-known cooler roAp group consisting of HR 1217, α Cir and 10 Aql, etc., all of which are multi-periodic, while HD 24355 is a single-mode pulsator. Another single-mode roAp star, HD 42659 (Martinez & Kurtz 1994), could have similar properties to HD 24355, although the position on the diagram depends on the uncertain quantity of L/M, and low-amplitude oscillations of HD 42659 are not well studied. The excitation mechanism of such supercritical high-order p modes is not known.

6 SUMMARY AND CONCLUSIONS

We have presented the first *Kepler* spacecraft observations of the high-amplitude roAp star HD 24355 alongside a detailed analysis of the ground-based discovery and follow-up photometric data. The *K2* data have allowed us to unambiguously determine the rotation period of the star to be 27.9158 ± 0.0043 d, a parameter which was uncertain when considering the ground-based SuperWASP data alone. Classification dispersion spectra allowed us to classify this star as an A5 Vp SrEu star.

Abundances derived from high-resolution spectra show HD 24355 to be slightly enhanced compared to some other roAp stars when considering the rare earth elements. However, a full and detailed abundance analysis is required to confirm its place amongst the roAp and noAp stars. The high-resolution spectra also allowed us to estimate a mean magnetic field strength of 2.64 ± 0.49 kG; however, we take this to be an upper limit on the value due to the lack of Zeeman splitting in the spectra, and the method used to derive that value.

There is a discrepancy between the $T_{\rm eff}$ of HD 24355 when using different methods to derive the parameter. Values from the literature, SED fitting abundance analysis and line fitting provide a wide range of $T_{\rm eff}$ values. However, we get the best agreement in results using solely the Balmer lines of both the low-resolution and high-resolution spectra, deriving 8200 ± 200 K, placing HD 24355 amongst the hotter roAp stars.

Analysis of the pulsation mode as detected in the *K2* data has shown the characteristic signatures of a roAp pulsator as predicted by the oblique pulsator model (Kurtz 1982; Bigot & Dziembowski 2002; Bigot & Kurtz 2011). The pulsational amplitude is modulated with the rotation period of the star, with the extremes in light variations and amplitude occurring at the same phase, indicative that the magnetic and pulsation poles lie in the same plane. The behaviour of the pulsation phase is not as expected, however. The very small phase change at quadrature is a surprise for a quadrupole pulsator. Examples from the literature (cf. Fig. 15) show a clear π-rad phase change when a different pulsation pole rotates into view, but this is not the case for HD 24355. Here we see a shift of only 1 rad at most.

Downloaded from http://mnras.oxfordjournals.org/ at Keele University on August 15, 2016

Table 12. Parameters of the roAp stars used to produce Fig. 19.

Star name	Main frequency (mHz)	Minimum frequency (mHz)	Maximum frequency (mHz)	Mass ($M_\odot$)	$\log(L/L_\odot)$	$\log(T_{\rm eff})$ (K)
HD 24355	2.596	2.596	2.596	2.00	1.28	3.910
HD 24712 (HR 1217)	2.721	2.553	2.806	1.65	0.92	3.860
HR 3831	1.428	1.428	1.428	1.76	1.09	3.884
HD 101065	1.373	1.246	1.474	1.53	0.77	3.806
HD 116114	0.782	0.782	0.782	1.92	1.32	3.903
HD 122970	1.501	1.501	1.501	1.48	0.79	3.840
α Cir	2.442	2.265	2.567	1.71	1.04	3.875
HD 134214	2.950	2.647	2.983	1.65	0.93	3.858
β CrB	1.031	1.031	1.031	2.10	1.40	3.908
33 Lib	2.015	1.803	2.015	1.78	1.16	3.869
10 Aql	1.448	1.366	1.469	1.85	1.25	3.875
γ Equ	1.365	1.228	1.427	1.70	1.10	3.878
HD 217522	1.200	1.200	1.200	1.49	0.85	3.816
K 8677585	1.660	1.458	1.676	1.80	1.20	3.863
HD 42659	1.718	1.718	1.718	2.10	1.48	3.900
HD 60435	1.381	1.381	1.457	1.82	1.14	3.910
HD 154708	2.088	2.088	2.088	1.43	0.73	3.829
HD 185256	1.613	1.613	1.613	1.40	0.68	3.853
K 10483436	1.353	1.353	1.512	1.60	0.84	3.868
K 10195926	0.975	0.920	0.975	1.70	1.00	3.857

This small 'blip' in the phase suggests that HD 24355 is pulsating in a very distorted mode, the most extreme case yet observed.

The rotationally split pulsation has provided us with the amplitudes to test the geometry of the star. As such, we modelled the system following the method of Saio (2005). Changing values of the inclination and obliquity angles and the polar magnetic field strength, and searching the parameter space surrounding our observational constraints, we conclude that HD 24355 is a distorted quadrupolar pulsator, with a magnetic field strength of about 1.4 kG. The model accurately matches the observed amplitude modulation of the pulsation, and the amplitudes of the rotationally split sidelobes. The pulsational phase variations are a stronger function of the evolution of the star, and as such provide a slightly greater challenge to model. We believe, however, that the model presented is a satisfactory match to the data, given our current observational constraints on the evolutionary stage of the star. We determine that the pulsation seen in HD 24355 is supercritical, making it the most precisely observed supercritical roAp star to date. The driving mechanism for such a pulsation is currently unknown, thus making HD 24355 a highly important target in understanding how some roAp stars can pulsate with frequencies well above the critical cut-off frequency.

ACKNOWLEDGEMENTS

DLH acknowledges financial support from the STFC via grant ST/M000877/1. GH is grateful for financial support from the Polish National Science Center, grant no. 2015/18/A/ST9/00578. This work is based on service observations made with the WHT operated on the island of La Palma by the Isaac Newton Group in the Spanish Observatorio del Roque de los Muchachos of the Instituto de Astrofísica de Canarias. The WASP project is funded and maintained by Queen's University Belfast, the Universities of Keele, St. Andrews and Leicester, the Open University, the Isaac Newton Group, the Instituto de Astrofisica Canarias, the South African Astronomical Observatory and by the STFC. This work made use of PYKE (Still & Barclay 2012), a software package for the reduction and analysis of *Kepler* data. This open source software project is developed and distributed by the NASA *Kepler* Guest Observer Office. We thank the anonymous referee for useful comments and suggestions.

REFERENCES

Asplund M., Grevesse N., Sauval A. J., Scott P., 2009, ARA&A, 47, 481
Babcock H. W., 1960, ApJ, 132, 521
Bakos G., Noyes R. W., Kovács G., Stanek K. Z., Sasselov D. D., Domsa I., 2004, PASP, 116, 266
Balmforth N. J., Cunha M. S., Dolez N., Gough D. O., Vauclair S., 2001, MNRAS, 323, 362
Balona L. A. et al., 2011a, MNRAS, 410, 517
Balona L. A. et al., 2011b, MNRAS, 413, 2651
Bertelli G., Girardi L., Marigo P., Nasi E., 2008, A&A, 484, 815
Bigot L., Dziembowski W. A., 2002, A&A, 391, 235
Bigot L., Kurtz D. W., 2011, A&A, 536, A73
Bruntt H. et al., 2008, MNRAS, 386, 2039
Buysschaert B. et al., 2015, MNRAS, 453, 89
Childress M. J., Vogt F. P. A., Nielsen J., Sharp R. G., 2014, Ap&SS, 349, 617
Cui X.-Q. et al., 2012, Res. Astron. Astrophys., 12, 1197
Cunha M. S., Alentiev D., Brandão I. M., Perraut K., 2013, MNRAS, 436, 1639
Droege T. F., Richmond M. W., Sallman M. P., Creager R. P., 2006, PASP, 118, 1666
Dziembowski W., Goode P. R., 1985, ApJ, 296, L27
Elkin V. G., Kurtz D. W., Mathys G., Freyhammer L. M., 2010, MNRAS, 404, L104
Elkin V. G., Kurtz D. W., Mathys G., 2011, MNRAS, 415, 2233
Evans D. W., Irwin M. J., Helmer L., 2002, A&A, 395, 347
Gray R. O., Corbally J. C., 2009, Stellar Spectral Classification. Princeton Univ. Press, Princeton, NJ
Handberg R., Lund M. N., 2014, MNRAS, 445, 2698
Handler G. et al., 2006, MNRAS, 366, 257
Hartman J. D., Bakos G. Á., Noyes R. W., Sipőcz B., Kovács G., Mazeh T., Shporer A., Pál A., 2011, AJ, 141, 166
Hatzes A. P., Mkrtichian D. E., 2004, MNRAS, 351, 663
Holdsworth D. L., 2015, PhD thesis, Keele University
Holdsworth D. L. et al., 2014a, MNRAS, 439, 2078
Holdsworth D. L., Smalley B., Kurtz D. W., Southworth J., Cunha M. S., Clubb K. I., 2014b, MNRAS, 443, 2049

Downloaded from http://mnras.oxfordjournals.org/ at Keele University on August 15, 2016

Howell S. B. et al., 2014, PASP, 126, 398
Høg E. et al., 1997, A&A, 323, L57
Kochukhov O., Ryabchikova T., 2001, A&A, 374, 615
Kochukhov O., Bagnulo S., Wade G. A., Sangalli L., Piskunov N., Landstreet J. D., Petit P., Sigut T. A. A., 2004, A&A, 414, 613
Kochukhov O., Alentiev D., Ryabchikova T., Boyko S., Cunha M., Tsymbal V., Weiss W., 2013, MNRAS, 431, 2808
Kurtz D. W., 1982, MNRAS, 200, 807
Kurtz D. W., 1992, MNRAS, 259, 701
Kurtz D. W., 2006, in Aerts C., Sterken C., eds, ASP Conf. Ser. Vol. 349, Astrophysics of Variable Stars. Astron. Soc. Pac., San Francisco, p. 101
Kurtz D. W., Shibahashi H., Goode P. R., 1990, MNRAS, 247, 558
Kurtz D. W., Martinez P., Koen C., Sullivan D. J., 1996, MNRAS, 281, 883
Kurtz D. W., van Wyk F., Roberts G., Marang F., Handler G., Medupe R., Kilkenny D., 1997, MNRAS, 287, 69
Kurtz D. W., Elkin V. G., Cunha M. S., Mathys G., Hubrig S., Wolff B., Savanov I., 2006, MNRAS, 372, 286
Kurtz D. W. et al., 2011, MNRAS, 414, 2550
Kurucz R., 1993, Kurucz CD-ROM No. 13. Smithsonian Astrophysical Observatory, Cambridge, MA
Lenz P., Breger M., 2005, Commun. Asteroseismol., 146, 53
Lüftinger T., Kochukhov O., Ryabchikova T., Piskunov N., Weiss W. W., Ilyin I., 2010, A&A, 509, A71
Lund M. N., Handberg R., Davies G. R., Chaplin W. J., Jones C. D., 2015, ApJ, 806, 30
Luo A.-L. et al., 2015, Res. Astron. Astrophys., 15, 1095
Martinez P., Kurtz D. W., 1994, MNRAS, 271, 118
Martinez P., Kurtz D. W., Kauffmann G. M., 1991, MNRAS, 250, 666
Mathys G., Lanz T., 1992, A&A, 256, 169
Medupe R., Kurtz D. W., 1998, MNRAS, 299, 371
Mkrtichian D. E., Hatzes A. P., Saio H., Shobbrook R. R., 2008, A&A, 490, 1109
Molnár L., Pál A., Plachy E., Ripepi V., Moretti M. I., Szabó R., Kiss L. L., 2015, ApJ, 812, 2
Monet D. G. et al., 2003, AJ, 125, 984
Montgomery M. H., O'Donoghue D., 1999, Delta Scuti Star Newsl., 13, 28
Moravveji E., 2015, in Meynet G., Georgy C., Groh J., Stee P., eds, Proc. IAU Symp. 307, New Windows on Massive Stars: Asteroseismology, Interferometry, and Spectropolarimetry. Cambridge Univ. Press, Cambridge, p. 182
Murphy S. J., Shibahashi H., Kurtz D. W., 2013, MNRAS, 430, 2986
Nardiello D. et al., 2015, MNRAS, 447, 3536
Niemczura E. et al., 2015, MNRAS, 450, 2764
Parsamyan E. S., Oganyan G. B., 1993, Astrofizika, 36, 501
Pepper J. et al., 2007, PASP, 119, 923
Pepper J., Stanek K. Z., Pogge R. W., Latham D. W., DePoy D. L., Siverd R., Poindexter S., Sivakoff G. R., 2008, AJ, 135, 907
Pojmanski G., 1997, Acta Astron., 47, 467
Pollacco D. L. et al., 2006, PASP, 118, 1407
Pyper D. M., Adelman S. J., 1983, A&AS, 51, 365
Ricker G. R. et al., 2015, J. Astron. Telesc. Instrum. Syst., 1, 014003
Saio H., 2005, MNRAS, 360, 1022
Saio H., 2014, in Guzik J. A., Chaplin W. J., Handler G., Pigulski A., eds, Proc. IAU Symp. 301, Precision Asteroseismology. Cambridge Univ. Press, Cambridge, p. 197
Saio H., Gautschy A., 2004, MNRAS, 350, 485
Savanov I. S., Malanushenko V. P., Ryabchikova T. A., 1999, Astron. Lett., 25, 802
Shibahashi H., Saio H., 1985a, PASJ, 37, 245
Shibahashi H., Saio H., 1985b, PASJ, 37, 601
Shibahashi H., Takata M., 1993, PASJ, 45, 617
Shortridge K. et al., 2004, Starlink User Note, 86
Skrutskie M. F. et al., 2006, AJ, 131, 1163
Smalley B., Smith K. C., Dworetsky M. M., 2001, UCLSYN Userguide. Available at: http://www.astro.keele.ac.uk/bs/uclsyn.pdf
Smalley B. et al., 2015, MNRAS, 452, 3334
Smart W. M., 1931, Text-book on Spherical Astronomy. Cambridge Univ. Press, Cambridge
Smith K. C., 1992, PhD thesis, University of London
Smith K. C., Dworetsky M. M., 1988, in Adelman S. J., Lanz T., eds, Elemental Abundance Analyses. Institut d'Astronomie de l'Univ. de Lausanne, Switzerland, p. 32
Smith A. M. S. et al., 2006, MNRAS, 373, 1151
Stibbs D. W. N., 1950, MNRAS, 110, 395
Still M., Barclay T., 2012, Astrophysics Source Code Library, record ascl:1208.004
Stoehr F. et al., 2008, in Argyle R. W., Bunclark P. S., Lewis J. R., eds, ASP Conf. Ser. Vol. 394, Astronomical Data Analysis Software and Systems XVII. Astron. Soc. Pac., San Francisco, p. 505
Takata M., Shibahashi H., 1994, PASJ, 46, 301
Takata M., Shibahashi H., 1995, PASJ, 47, 219
Torres G., Andersen J., Giménez A., 2010, A&AR, 18, 67
Udalski A., Szymanski M., Kaluzny J., Kubiak M., Mateo M., 1992, Acta Astron., 42, 253
Ulaczyk K. et al., 2013, Acta Astron., 63, 159
Unno W., Osaki Y., Ando H., Saio H., Shibahashi H., 1989, Nonradial Oscillations of Stars. Tokyo Univ. Press, Tokyo
Vanderburg A., Johnson J. A., 2014, PASP, 126, 948
Wade G. A., Leblanc F., Ryabchikova T. A., Kudryavtsev D., 2003, in Piskunov N., Weiss W. W., Gray D. F., eds, Proc. IAU Symp. 210, Modelling of Stellar Atmospheres. Astron. Soc. Pac., San Francisco, p. D7
Zhao G., Zhao Y.-H., Chu Y.-Q., Jing Y.-P., Deng L.-C., 2012, Res. Astron. Astrophys., 12, 723

This paper has been typeset from a TEX/LATEX file prepared by the author.

Downloaded from http://mnras.oxfordjournals.org/ at Keele University on August 15, 2016